MASS BALANCE OF NYAINQEN TANGLHA GLACIER, TIBET, 1977 TO 2001, DERIVED BY TOPOGRAPHICAL MAPS AND SATELLITE IMAGES

Master Degree Thesis in Meteorology

Cai Dong
May 2004

Geophysical Institute
University of Bergen

Abstract

NyainQen TangLha Glacier plays an important role in the Tibetan plateau's climate system. Because of high altitude, steeply sloping terrain and difficult access, regular, systematic surveys of glacial variation are almost impossible in most regions of the glacier. As a result, satellite images are a convenient tool for studying the mass balance of the glacier, allowing us to conduct research over steep and otherwise inaccessible areas.

This paper studies the mass balance of the NyainQen TangLha glacier area (30°15'N, 90°10'E, 5000-7000 m a.s.l. some 100 km to north-west of Lhasa.) in the Tibet Autonomous Region during the last few decades and investigates possible future glacial variations due to climate change. The aim is to examine variations in the terminus of different glacial tongues of the main glacier. The study is based on a comparison between an original topographic map produced in the earlier USSR in 1977 and satellite images from band 9 of ASTER in November 2001. Examining these two sources shows a negative change in the mass balance of all glacial tongues in the region. This study discusses the reasons for this with respect to changes in ablation, in accumulation.

Contents

Preface

During the past decades, many remote-sensing techniques have been applied in the study of glaciers. For example measurements of absolute ice thickness have been made using radio-echo sounding from surface and airborne platforms. Changes in surface elevation over time have been recorded using aerial photogram-metric methods as well as geodetic airborne or space-borne radar and laser altimetry. Moreover delineation of the surface expression of glacier faces and measurement of fluctuations of the termini of valley glaciers and outlet glaciers (Williams and Hall, 1997) has been carried out using satellite sensors. Furthermore, satellite remote sensor studies of glacier fluctuation have been conducted in areas where persons have been unable to reach and measure ground data.

The earth's smaller glaciers have generally been receding during the 20th century (Haeberli and Beniston, 1998). This has been accompanied by an estimated 1-3 mm/a rise in sea levels (Warrick, 1996), perhaps as much as one-third of which has been caused by volume reduction in glacial ice primarily from south-eastern Alaska (Meier, 1984). The terminus-position changes of small glaciers often shows a response time of a decadal time-scale, because smaller glaciers react more rapidly to climate change than the larger ice caps (Haeberli, 1995). In general, however, glaciers with a negative mass balance will retreat over time, although large and relatively flat glaciers have a tendency of down-wasting rather than retreating in the case of rapid warming (Haeberli and Hoelzle, 1995).These have provided the impetus for my project.

Acknowledgements

First of all I would like to express my gratitude to my advisors Yngvar Gjessing and Knut Barthel. They gave me an interesting opportunity to explore mass balance of NyainQen TangLha glacier in Tibet and were an invaluable help throughout the long process. Without whose help I would never have been able to complete this project. I would especially like to express my gratitude to my advisor and best friend Yngvar, who has been of inestimable help. Whenever I reached a hurdle in this project, he was able to help me overcome it. He has also spent an enormous amount of time and energy throughout my three years life in Norway.

I would like to thank everyone at the geophysical institute for their help. Asgeir, Jan Asle and Knut Frode who have been big supports and for providing the meteorological and radiation data and for always taking the time to answer my questions.

In addition, I want to thank the network for University Co-operation Tibet-Norway and its main members Yngvar, Torstein and Benter at the University of Bergen, for giving me this opportunity and supporting me throughout my master course. Had it not been for them, I may never have had the opportunity to get acquainted with Svalbard, Bergen, and get such a stimulating introduction to glaciology and remote sensing.

Last, but not least, a great thank you to all my family and hometown friends also living in Bergen. The biggest thank you to my dear wife Qiangzong Trarong and my smart daughter SonamYangzong Telab for always being there for me.

Caidong Telab
Bergen, May 2004

Chapter 1

Introduction

The objective of this master thesis is to study glacial changes on Mount NyainQen TangLha (30°15'N, 90°10'E, 5000-7000 m a.s.l. and 100 km to north-west of Lhasa.) in the Tibet Autonomous Region during the last few decades and to investigate possible future glacial variations due to climate change. The study was based on a comparison between an original topographic map produced in the earlier USSR in 1977 and satellite data from ASTER from November 2001. The aim is to examine the terminus of fifteen glacial tongues of the glacier of NyainQen TangLha.

1.1 A brief description of the glacial conditions in Tibet

Much of the Tibet Autonomous Region is mountainous. The rough topography with great differences in elevation and steeply sloping terrain means that the region is exposed to various natural hazards including landslides and river erosion. In addition, the area is exposed to other hazards such as flooding which can occur when glacier dammed lakes are drained under their ice dams or basally frozen dams are overflow or the moraines burst. Some areas higher than 4.000 meters above sea level are covered by snow and ice throughout the year. Many glacial lakes may be created when the glaciers melt. For example, four of Tibet's largest lakes, NamTro, YanZhuo YumTro, MarPan YumTro, and YugonTro which have been formed in this manner. Glacial lakes are also the headwater source of many great rivers in the region such as the two largest rivers, the YarLung Zangbo and the NuanQiu Zangbo. Most of the glacial lakes are located lower down in the valleys at the margins of the glaciers. They are formed by the accumulation of vast amounts of water from the melting of the snow and ice cover and are blocked at their ends by moraines. Many small lakes have developed in the western part of Tibet and this may be attributable to the effects of recent global warming (Jiejun 1986).

1.2 A brief description of NyainQen TangLha

1.2.1 Geographic position

The NyainQen TangLha is a mountain range that runs 740 kilometres from west to east in the middle part of the South Tibetan Plateau. It joins the Gangku Kanchi Mountain in the west, and extends south-eastwards to the Baxoila Ling peak of the Heng-duanLha range whose centre wells northward. The NyainQen TangLha range serves as the watershed for two major water systems that is the YarLung Zangbo and the Nuanqiu Zangbo rivers which divide the Tibet Autonomous Region into three large regions; North, South and Southeast Tibet. As early as the in Tertiary and Quaternary Periods, the area of NyainQen TangLha was controlled and pressed by the Nuanqiu fracture belt and the Yarlong Zangbo fracture belt which run east to west. Consequently the area of NyainQen fractured, folded and rose violently forming the huge mountain range reaching 6000 m above sea level (Jiejun 1986).

The main peak of the NyainQen TangLha has a height of 7048 m. This peak lies in Damxung County of the Tibet Autonomous Region. NyainQen TangLha has an arid climate as it lies in the hinterland of the continent and is screened by mountains. The annual precipitation of this area varies between 200 and 400 mm (Jiejun and Zhengxing 1986). Fig 1-1 shows a map which was taken from the internet (map of Tibet 2003). It shows the position of NyainQen TangLha in Tibet.

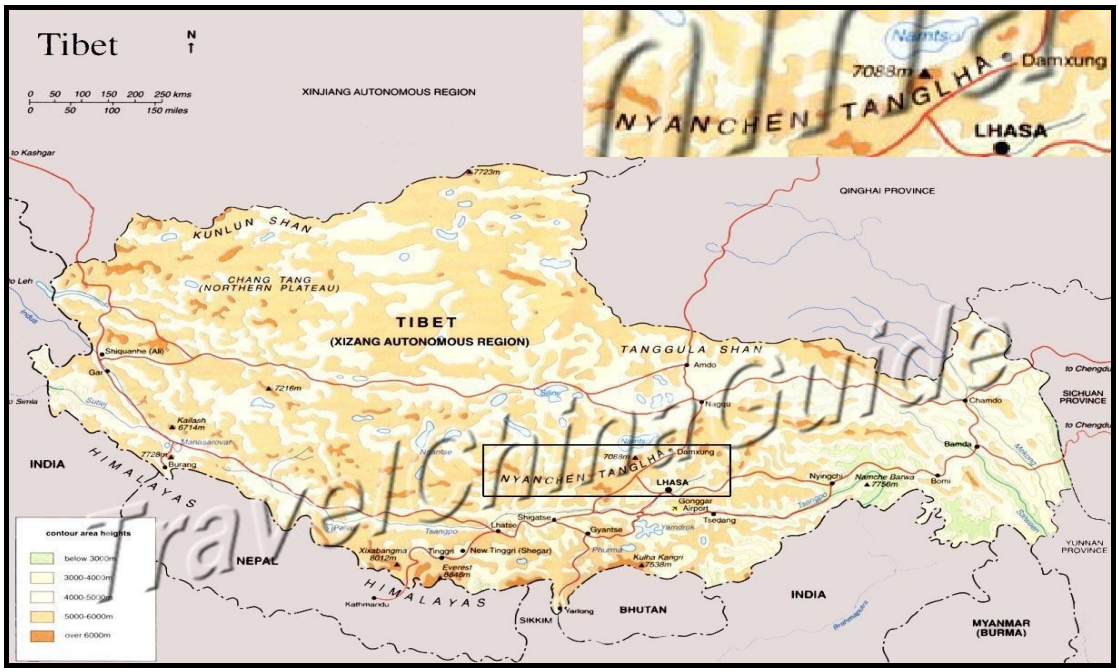

Fig 1-1: Map of Tibet. The NyainQen TangLha range is marked, and enlarged (map of Tibet 2003) in the top right –hand corner.

1.2.2 classification of glaciers to derive type of NyainQen TangLha glacier

Ahlmann (1935a) proposed a 'geophysical' classification of glaciers according to ice temperature and amount of surface melting. Three categories which also refer to the geographical location of the glacier on the Earth were established that are still used today:

1. *Temperate glaciers*
2. *Polar or cold-base glaciers*
3. *sub-polar glaciers*

According to Harrison, (1972) a *temperate glacier* is approximately at the pressure-melting point throughout its thickness, except for 10-15 m just below the surface, which may be colder during the winter. Ice temperature decreases downward at a rate of about $0.06^{0}C/100m$ as a result of the effect of increasing pressure on the melting temperature. Thus, ice may coexist with water at temperature below $0^{0}C$ near the base of a glacier. All heat goes into the melting of ice (as opposed to ice below the pressure-melting point where heat must be added to bring the ice to the melting point). Thus, melt-water is commonly found throughout the thickness of the glacier. This fact allows more rapid conversion of snow and firn into ice and also increases the plastic deformation of the ice. As a result, flow rates in temperate glacier are greater than cold, polar glaciers. Temperate glaciers are also referred to as *wet-based glaciers* because of the common occurrence of melt-water at the base of the glacier, which increases the sliding of ice over its bed. Thus, basal sliding is a more important factor in temperate glaciers but absent in cold based polar glaciers. The production of much melt-water also leads to the building of large outwash plains in front of the glacier (Easterbrook 1999).

Ice in *polar or cold-based glaciers* is entirely below the pressure-melting point of ice; Heat goes into raising the temperature of the surface layer in summer season but it remains frozen at the end of the summer (Hooke, 1977). In such glaciers, negligible melting occurs and the conversion of snow and firn to ice takes many times longer than in temperate glaciers. In addition, ablation takes place only by calving, wind erosion, or sublimation. Glacier velocities are considerably slower than in temperate glaciers. Because ice in the basal portions of polar glaciers is below the pressure-melting point, melt-water is absent and the ice is frozen to the

bedrock surface. Basal sliding is thus absent, and glacial motion is only by deformation. Such glaciers are not effective in eroding the sub-glacial bedrock floor by sliding. The lack of melt-water results in the absence of outwash plains. (Easterbrook 1999)

Sub-polar glaciers are often frozen to their bedrock, as the case for polar glaciers, but surface melting occurs in summers and they may be temperate in the accumulation area. Thus, they are intermediate between temperate glaciers and polar glaciers, possessing some characteristics of each. In the accumulation area the melt water will ice freeze in the snow below and forms are isothermal layer in summer. Thus snow has low conductivity compared the ice in the ablation zone and they reduce the cooling winter. (Easterbrook 1999.)

It is argued that according to the classification outlined above, the NyainQen TangLha can be classified as temperate glacier. However, and more significantly, it also has characteristics that closely relate it to a sub-polar one. The reason we can place this particular glacier in the sub-polar category is that evidence shows that temperatures at the base of the glacier can reach below the melting point during the winter months. There is no technical data for this, but in my field work and through the reports of local inhabitants, streams that are present in the summer can not be found in the winter months. An explanation for this appears to lie in the unusual degree of thinness of this glacier as compared to, for example, the Nigardsbreen temperate glacier in Norway. The thinner the glacier is, the more rapid and noticeable the effects of heat flux become. The temperature of the glacial ice of a thin glacier, easily changes with earth's surface air temperature, and consequently this maintains the glacial temperature at around the melting point in summer time and below the melting point in winter.

1.3 A brief description of the reciprocal effects of the NyainQen TangLha to global climate and global climatic warming to the NyainQen TangLha

According to a Tibetan saying, the Tibetan Plateau is the third polar area of the earth. Here, even small climactic variations will dramatically influence the global climate situation. This polar region is the source for rivers that flow down to half of the population on earth; the Yellow River and the Yangtse. These two major rivers originate in north eastern Tibet and flow across China. The Mekong also starts in eastern Tibet and traverses down to Burma. In

addition, most of the major rivers in Nepal originate in the Tibetan plateau. None of these rivers run dry in the summer as a result of the snow melting on the glaciers of the Tibetan plateau in the dry summer season. The Tibetan plateau has an influence on world climate. The elevation of the plateau cuts the jet stream in half during the northern winter, and it is the northward movement of the jet stream in spring that allows the monsoon rains to gradually push it into the South Asian subcontinent (Kang 1996). Consequently, one can determine the essential role that the NyainQen TangLha, as the second largest mountain range in the Tibetan plateau, plays in the global climate scene.

A report (Hansen 1999) by researchers at the NASA Goddard Institute for Space Studies who analyzed data collected from several thousand meteorological stations around the world stated: "the global average surface temperature is likely to be about 0.32 °C above the climatological average for the period 1961-1990. It was increasing from 1990-1999 and 1990, 1991, 1995, 1997 were warmer years and 1999 was one of the warmest years. As a new century begins, the global mean temperature is 0.6 °C above those at the start of the 20th century" (www.giss.nasa.gov/reseach/observe/surftemp/.) Fig 1-2: Illustrates the trend of global annual surface temperature relative to 1951-2000 mean. (This is derived from a 2002 summation.)

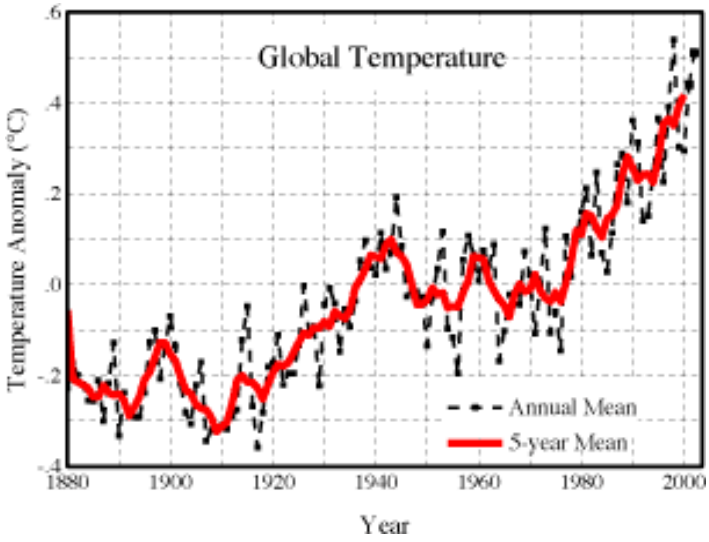

Fig 1-2: Mean anomaly of mean air temperature of the earth as a function of time (Hansen 2001). From the chart, one can see that the warmest temperature occurred in 1998, while the third warmest year was 2001.

It appear that Tibet is not an exception from the worldwide warming pattern and evidence of this can be found in records of Lhasa's annual air temperature which shows that the city has experienced an annual warming in the period between 1950 and 1990 of approximately 0.17°C/decade. Fig 1-3 shows the variation of the annual mean air temperature in Lhasa the last 40 years (Wang Lha, 2003). It is also important to note the NyainQen TangLha is only 98 km from Lhasa. Consequently a large scale increase in air temperature may be one of the reasons why the glacial tongues have been retreating.

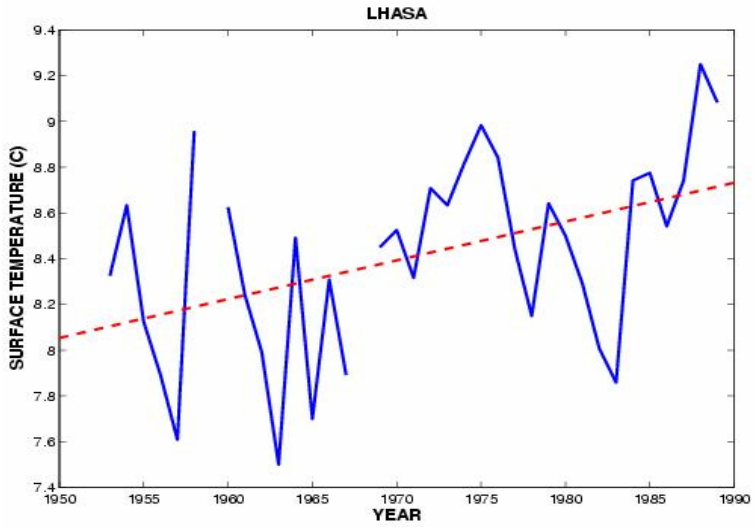

Fig 1-3: Mean annual air temperature and long-tem trends for Lhasa given in Celsius/decade (Wang La, 2003)

Chapter 2

Data sources and methods

2.1 Data sources

Two set of data sources were used. The first was a topographical map produced in the earlier USSR in 1977 which is illustrated in Fig 2-1. The topographic map was made from aerial photographs with 40 m contour intervals. The accuracy in the given position of the glacier margins as shown on the maps is considered to be ± 100 m. The second was ASTER data from the year 2001.

2.1.1 Topographical map

The topographical map was scanned and divided into 4*4 km cells and the following were used to compile the inventory of Table 2-1.

Table 2-1: Inventory topographic map source

Sours	Scale	Number	Date	Coverage
Topographic map	1:200 000	08-46-13	1977	90E-91E 30N-30.67N

Fig 2-1: The topographic map

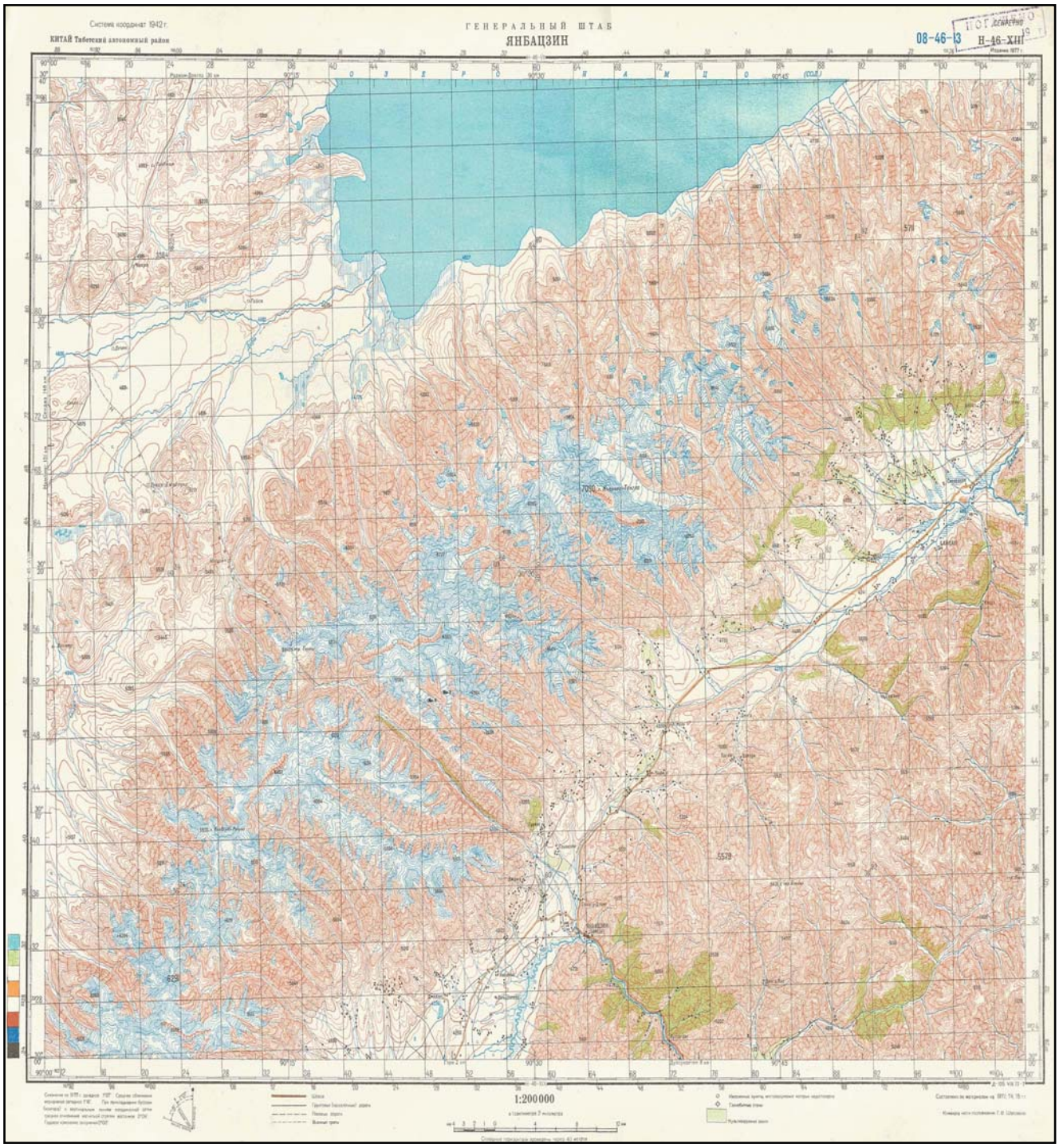

2.1.2 ASTER data

ASTER overview

ASTER stands for the Advance Space-borne Thermal Emission and Reflection radiometric radiometer. It is an imaging instrument (essentially a large digital camera) bolted to the Earth Observing System flagship satellite called Terra (which is Latin for land) which was launched on December 18, 1999. There are five instruments on Terra; ASTER, CERRES, MISR, MODIS and MOPITT. The satellite operates in a circular, near polar orbit which is sun-synchronous with equatorial crossing at a local time 10.30 a.m. and repeats this cycle every sixteen days.

The Instrument

ASTER takes about 600 pictures ("scenes") a day, each covering an area of 60 x 60 km. Like most satellite sensors, ASTER is much more complex than a hand-held digital camera. First, and most importantly, a separate image is created for each colour (or more precisely, each wavelength range, ¨band¨). Because ASTER has a total of 14 bands, each scene is compiled of 14 different images. This is useful because different materials can look very different in different bands.

Another difference between ASTER and a typical digital camera is that ASTER has three lenses instead of the usual one, and these lenses are referred to as “telescopes” because of their size and power. In fact, ASTER is really three instruments, each one specializing in a different part of the spectrum. This is because photons in one part of the spectrum behave very differently than the photons in another. Consequently different technologies are used for each part of the spectrum.

One of the most important characteristics of ASTER is; (1) a wide spectral range and a high spectral resolution. (2) 15m (visible and near infrared spectral region), *30m (short-wave infrared spectral region),* and 90m (thermal infrared spectral region) spatial resolutions. More significantly ASTER’s high resolution is beneficial to the study of the detection of changes in the surface condition of the NyainQen TangLha glacier (Abrams, (2000).

The ASTER instrument and its operation is a joint project between the US and Japan. Japan designed and built the instrument, the processing system, and the operations system,

and performs data processing. The US designed, built, and now operates the Terra spacecraft and the associated ground system.

The ASTER is a multi-spectral sensor and is comprised of a set of three subsystems; the VNIR, SWIR and TIR, respectively. Our data was obtained from the SWIR (Short Wave Infrared Spectral Region) subsystem.

The SWIR subsystem uses a single aspheric refracting telescope. The detector in each of the SWIR's six bands is a Platinum Silicide-Silicon (PtSi-Si) Schottky barrier linear array cooled to 80K. Cooling is provided by a split Stirling cycle cryocooler with opposed compressors and an active balancer to compensate for the expander displacer. The on-orbit design life of this cooler is to be 50,000 hours. Although ASTER will operate with a low duty cycle (8% average data collection time) the cryocooler will operate continuously because of the long cooling and stabilization time. No previous cyrocooler has demonstrated this length of performance and the development of this long-life cooler was one of several major technical challenges facing the ASTER team (Arai, 2001).

The cryocooler is a major source of heat. Because the cooler is attached to the SWIR telescope, which must be free to move to provide cross-track pointing, this heat cannot be removed using a platform provided cold plate. This heat is transferred to a local radiator attached to the cooler compressor and radiated to space (Arai, 2001).

The system signal-to-noise is controlled by specifying the NE[1] $\Delta\rho$ that varies from 0.5 to 1.3% across the bands from short to long wavelength. The absolute radiometric accuracy is 4% or better. The combined data rate for all six SWIR bands, including supplementary telemetry and engineering telemetry, is 23 Mbps (Arai, 2001).

The Images

All digital images, whether from personal digital cameras or from those in space, are composed of pixels (picture elements). Each ASTER image 16 million pixels (4200 x 4200), and is a "composite" colour image derived from *bands 9* which is sensitive to middle-infrared. Each pixel in this image corresponds to about a *30 x 30 m* patch on the ground. Because of the substantial amount of compression required to reduce the file size the images used in this thesis have unfortunately suffered from a reduction in quality.

[1] NE stand for noise-equivalent

In the images *snow/ice/water is very dark.* Living vegetation appears red. Man-made materials like concrete and buildings tend to be a light blue or grey. The colour and the brightness depend on the composition of the materials it is made and their reflectance. One can see these, sometimes dramatic differences in Fig 2-2 which shows reflectance of ice, snow, salt water, rocks, brown sandy loam and construction concrete.

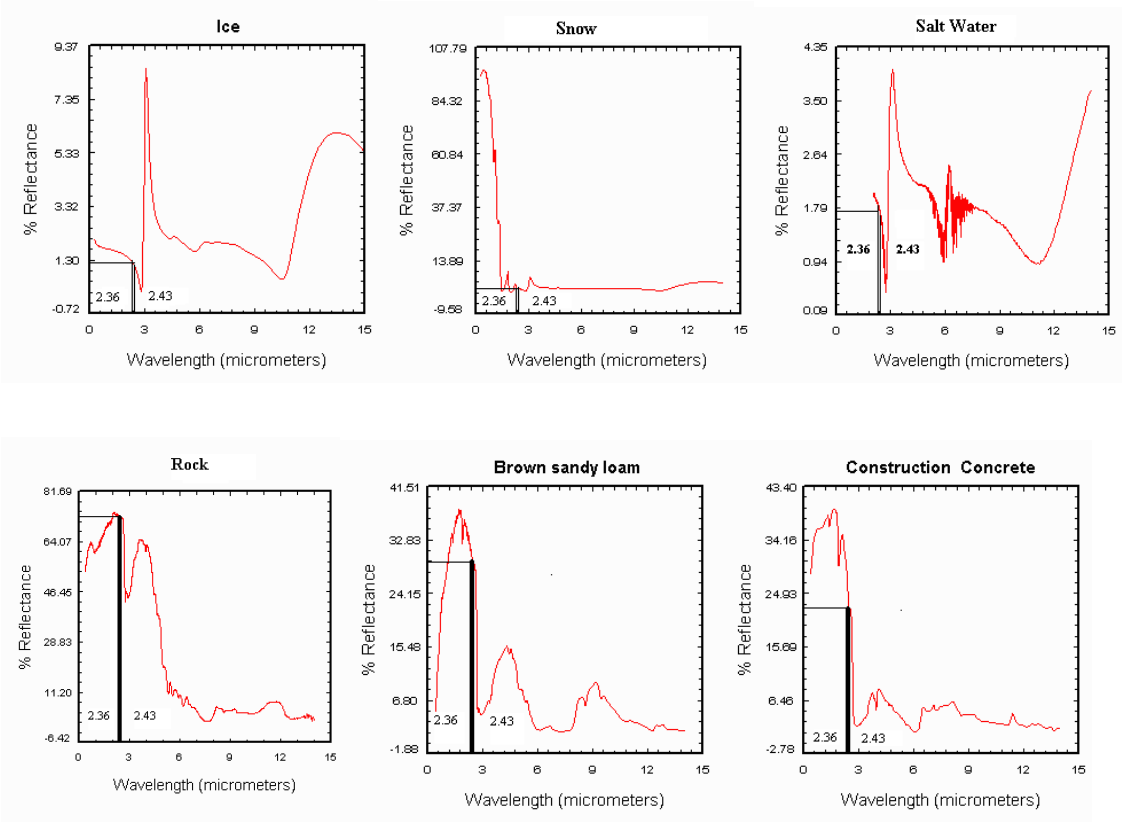

Fig 2-2: Shows reflectance to the six kinds of varies material (http://speclib.jpl.nasa.gov/Search.htm).

We may ask why the scenes are not displayed in their natural colours, and there are several reasons for this. The first is due to the fact that the human eye cannot see infrared, yet some visible colour has to be used to represent it if the images are going to be useful. For infrared-sensitive film, that colour was red. Red has therefore been used to represent the infrared ever since, even for digital images that use no film, such as ASTER.

The second reason is that ASTER does not have a band that detects blue light (this is because blue light tends to be scattered much by the atmosphere), so a real "natural colour"

image is not possible. Although natural colour can be simulated using some image processing tricks, it is rather difficult to automate those tricks in order to create consistently good images.

The third reason is that the colours have been assigned due to the existence of several different bands, each needing colours to be assigned to wavelengths the human eye cannot see. For example, band 9 is sensitive to middle infrared spectrum and thereby has been assigned the red. Therefore, the more a piece of ground reflects this band, the brighter the red colour will be on the images.

Inventory data source in our studying

The SWIR has 6 difference bands from 6 to 11. However, *band 9* is of primary interest for this study. The following data sources were used to compile the inventory of table 2-2.

Table 2-2: Inventory Aster data source

Source	Band	Spectral range (**μm**)	Radiometric resolution (**$Wm^{-2}sr^{-1}\mu m^{-1}DN^{-1}$**)	Spatial Resolution (**m**)	Date
ASTER-data	9	2.360-2.430	0.0318	30	20.11.2001

2.1.3 Coordinate systems

Three coordinate systems were applied in the processing of the data:

1. Satellite image coordinate system given by lines and pixels (abbreviated L/P). Lines are counted from north to south and pixels from west to east. One unit is equal to 30 m in the terrain.
2. Map coordinate system given by kilometres northwards and eastwards (abbreviated N/E).
3. Geographical latitude and longitude in degrees (abbreviated L/L).

Three Matlab functions have been edited in order to carry out the transformations work between the various coordinate systems.

The function ***geolaloswi****r* computes the latitude and longitude for a selected position on a satellite image given by line and pixel number. The function applies the geolocation field following the ASTER data (latitude and longitude for each 210^{th} line and each 249^{th} pixel are given in the *g*eolocation field), and carry out a linear interpolation between the geolocated points surrounding the selected position.

The function ***geogrid*** computes the map coordinates for a selected pair of latitude and longitude values. The grid position values of the four corners of the map have been carefully determined. The function computes the grid position values of the selected pair of latitude and longitude by linear interpolation between these corner points.

The function ***asterpoint*** computes the latitude and longitude for a selected pair of map coordinates, and thereafter uses these latitude and longitude values to determine the line and pixel values of the corresponding point on the satellite image. The first step is an inversion of the ***geogrid*** function, while the second step is an iterative procedure using a function similar to ***geolaloswir***.

We can see Fig 2-3 that shows the interrelation of the three coordinate systems.

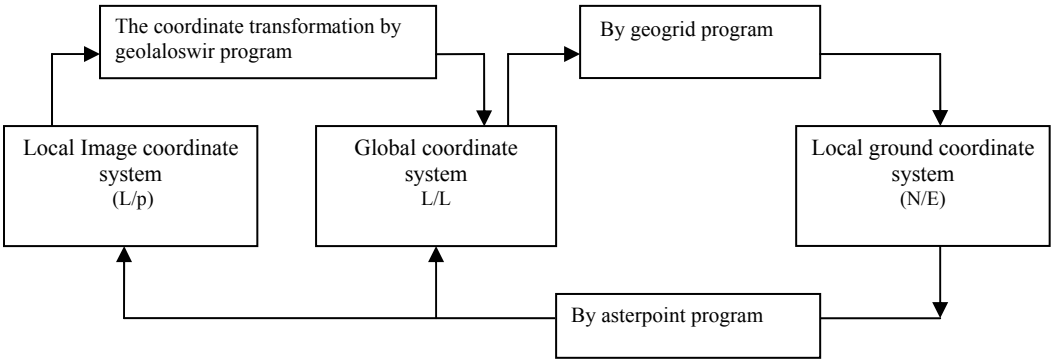

Fig 2-3: Coordinate Transformations

2.1.4 Swirsubreg and Polyarea program

The running of the ***swirsubreg*** program consists of loading the band 9 the ASTER data and inputting line and pixel number ranges for a selected area. A contour plot of the short wave IR irradiation values of the selected area is then plotted by the matlab program. The range of the pixels is by 0-2489 and runs from west to east. The range of lines is by 0-2099 and runs from north to south.

Polyarea stand for area of a polygon and is a matlab program which is used to calculate the area of glacial tongues. The area of a glacial tongue is specified by the vertices in the vectors eastward and northward of the map coordinate system. A polygon is created using a finite number of points around the glacial tongue. None of the sides of the polygon must intersect. If they do, the absolute value of the difference between the clockwise encircled area and the counter-clockwise encircled area is calculated by *polyarea.*

2.2 Methods of data preparation and process

The raw data from the original topographical map required some form of conversion in order to be able to be compared with the ASTER data. The first step of the conversion process was to subdivide the original **4 * 4**km cells imposed onto the scanned map into smaller, more limited cells. The large cells made the determination of specific terminus points

of the glacial tongues impossible. The geographical map with latitude and longitude or map coordinate system that given by kilometres northwards and eastwards was then transformed by a matlab program (Asterpoint) to satellite image coordinate system, corresponding to the ASTER satellite data.

The Aster-data was used to plot the extent of the NyainQen TangLha glacial tongues which was done by employing the matlab program (Swirsubreg). The first phase of processing the ASTER data entailed defining the ice limit pixel. Secondly, these limits needed to be compared with those defined by the topographical map in addition to the field work data collected in Tibet during summer 2003.

A digital image is a picture represented by numbers. The image is given as a matrix where each element represents an area of 30-by-30 square meters. The row number of this matrix is equal to line number and pixel number one, the column number is equal to pixel number plus one. Associated with each pixel is a numerical value often denoted data number (DN) which quantifies the average radiance (brightness or grey-tone). Possible DN values range from 0 to 255 due to a signal quantization level of 8 bits (Landmark, 1996). Defining the ice limit means determining a probable DN value within the 2.36-2.43 μm band which is the band used in this study.

.

Fig 2-4 shows a very low irradiance of snow/ice within 2.36-2.43 μm. This can indicate an even lower DN value. According to this relationship, we have researched possible DN values from 10 to 100 in all the various areas of NyainQen TangLha glacier where ASTER data was also available. The most probable DN limiting value was then chosen to be 60.

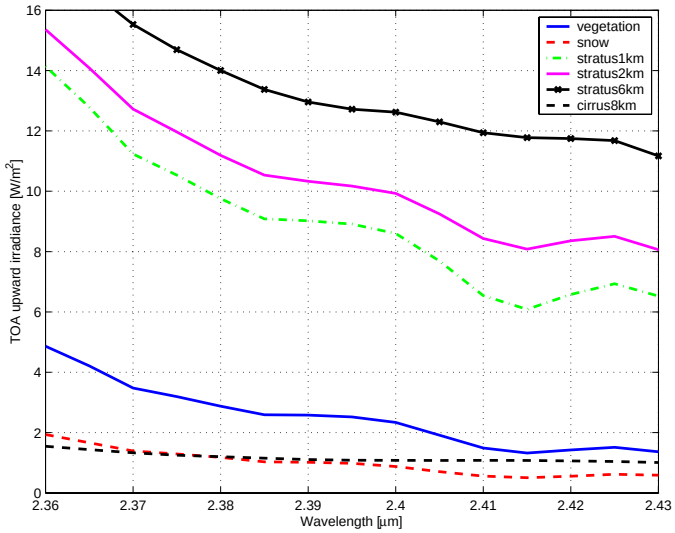

Fig 2-4: Shows total upward irradiance (**$Wm^{-2}\mu m^{-1}$**) of snow with the wave-length **(µm)** (K. F. Dagestad, pers.comm.).

Reasons to choose the DN value representing the ice limit equal to 60:

(1) A similar irradiance was observed between NumTro Lake (the biggest glacial lake in Tibet which is fed by the NyainQen TangLha glacier and is around 5000 m above sea level) and the glacial tongues number 1 and 2, two of the tongues that have been studied. The edge of NumTro and both the glacial tongues number 1 and 2 are located where the line and pixel number range in *swirsubreg* are 800-1000 and 400-800, respectively. From Fig 2-5 we see that the lake and the glacier tongues have the same DN-values. As the data was collected by the ASTER sensor on November 20, NumTro's edge could have been covered by snow/ice. It has been quoted that NumTro could very well be frozen over at the beginning of November (Shengtang, 1984). After some testing we estimated the most probable DN value representing the ice limit to be equal to 60.

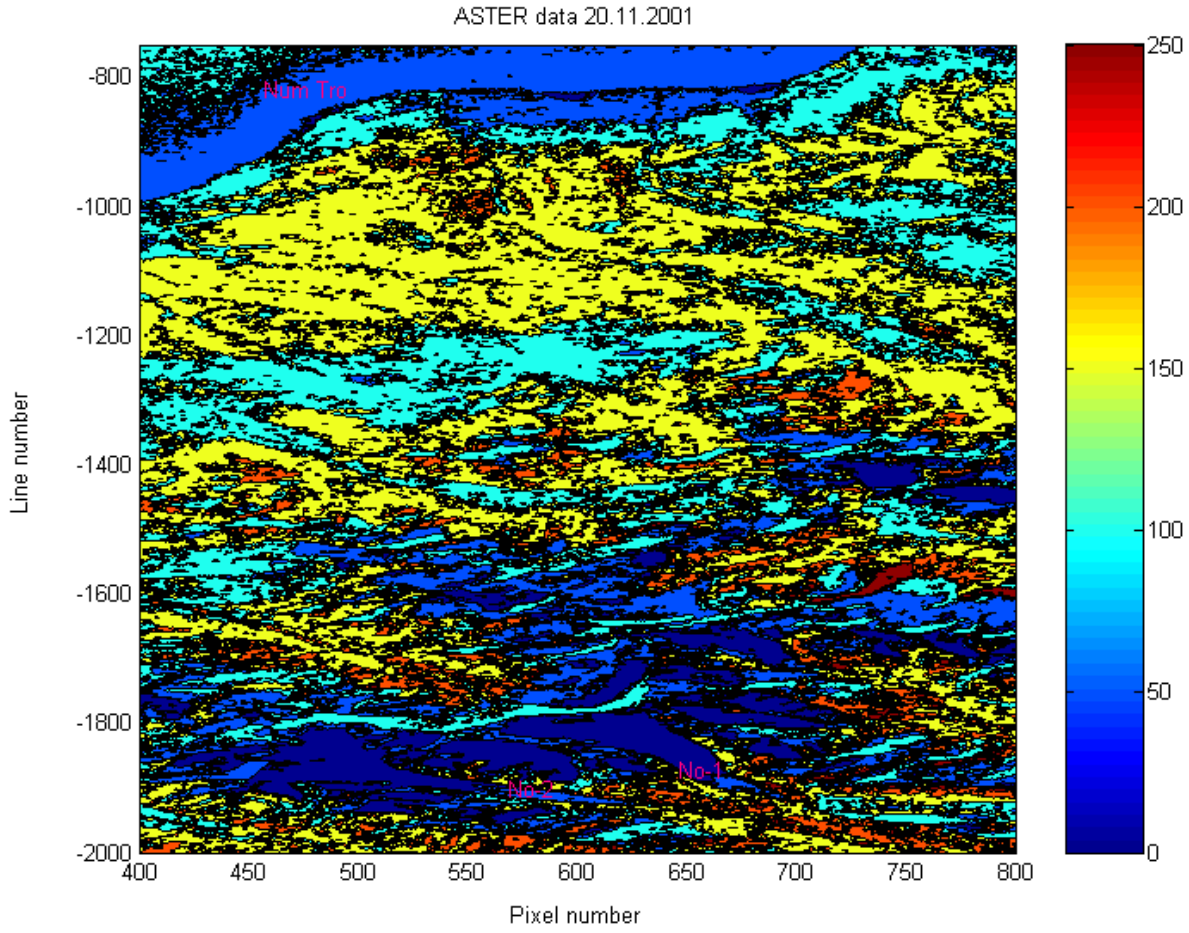

Fig 2-5: The DN values for the edge of the lake appearing in the upper part of the figure and thetwo glacial tongues in the lower part of the figure which are equal to **60**.

(2) According to the ASTER data, the topographic map, local topographic maps and by GPS information the glacial tongues No-1 and No-2 of the NyainQen TangLha glacier were located. The image of the two glacial tongues which after Aster data was plotted by matlab program are strongly coincide with the true position of the two glacial tongues that were observed in field work in July 2003. This can be also evidence for chosing the probable DN value of 60.

(3) The possible DN value was calibrated by a method of further comparison: 1. More than 20 points were chosen on the contour of each tongue within the image. 2. These points were transformed from satellite image coordinates to geographical latitude and longitude. 3. They were marked on the topographical map. We then measured and observed the situation of overlap between these points and the contours of the two original glacial tongues on the topographical map, estimated from several DN value calibaration. We defined the ice limit pixel or the probable DN value of 60.

Chapter 3

Results

3.1 Changes in the glaciers of the NyainQen TangLha region

Primarily small glaciers and low elevation glaciers have retreated, some of even disappeared and all remain of the original glacier in August 2003 are definitive traces on the bedrock over which the glacier once flowed. See figures Fig 3-1 and Fig 3-2. According to a local seventy-two year old herdsman named Droma, these changes have take place in what he estimates to be the past twenty years.

Fig 3-1: Distinct indications of glacial retreating. This mountain is located just outside the town of YanBaJing. It is in the eastern part of the NyainQen TangLha range**.**

Fig 3-2: The colour of rock-debris, left by the retreating of the glacier that originally extended to the other side of YanBaJing can clearly be seen. The photograph is taken in the northern part of NyainQen TangLha range.

3.2 Comparison of satellite-derived data and the topographical map to define the termini of glacial tongues

We measured fifteen different glacial tongues on the NyainQen TangLha glacier. Changes in their termini positions and area of their tongues were computed by comparison between the 2001 ASTER data and the 1977 topographical map. The comparison period spans twenty-four years. An equal sided square was drawn over the termini of the 1977 glacial tongues. The corner points were named a, b, c, d with the termini (T) located in the centre. An asterpoint program was used to translate points a, b, c, d to the local image coordinate system. The termini were located within the centre of these transformed points a`, b`, c`, d`. (Fig 3-3)

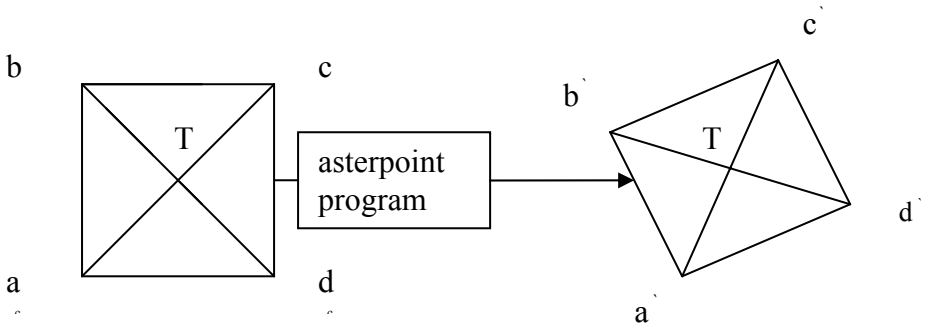

Fig 3-3: The determination of the terminus of the glacial tongue

The fifteen glacial tongues were separated into two groups because of the difference in the extent of the receding in the two parts of the region. Eleven of the glacial tongues in the southern part of NyainQen TangLha glacier constituted one group hereafter referred to as group A. Four other tongues in the northern part of the glacier comprised the second group, subsequently called group B. All fifteen tongues have been marked and summarized in Table 3-1 to 3-8. In addition, there are ten figures (plotted by the matlab program) and ten corresponding maps (cropped from the topographical map,) which relate to these tables.

(1) Group A subdivided into three groups according to directional flow

Seven of the eleven glacial tongues have a flow direction from northwest to southeast. These were numbered 1 through 7. All the appropriate data concerning these tongues are collected in Table 3-1 to 3-4.

The flow direction of two other glacial tongues is from north to south and these were numbered 8 and 15, respectively. Data for these two tongues are collected in Table 3-5.

Tongues numbered 9 and 14 flow from west to east and their data is collected in Table 3-6.

(2) Group B subdivided according to directional flow

Two of the glacial tongues in this part of the region flow from southeast to northwest. These were numbered 10 and 13, respectively, and data for both are collected in Table 3-7.

The other two glacial tongues in this group, numbered 11 and 12, have a flow direction from south to north. Data for these has been collected in Table 3-8.

Table 3-1: Comparison of original and present termini positions for tongues No-1 and No-2. Distance and area of receding calculated. (IX stands for pixel number, IY stands for line number a, b, c and d are the corner points of the terminus. One pixel size equals 30 m)[2].

	Outlet number	IX	IY	Latitude	Longitude	Geo-north	Geo-east	Receding values
Original terminus	No-1							
a		715	1981	30.2275	90.3991	48.2600	51.2500	
b		714	1974	30.2295	90.4162	48.5100	51.2500	
c		722	1971	30.2300	90.4188	48.5100	51.5100	
d		724	1979	30.2277	90.4190	48.2600	51.5100	
Present terminus								**-2929m** and **-2.5 km^2**
a		647	1877	30.2582	90.4004	51.6861	49.8098	
b		671	1877	30.2571	90.4078	51.5538	50.5197	
c		671	1902	30.2507	90.4066	50.8425	50.3852	
d		647	1902	30.2564	90.3991	50.9750	49.6750	
Present terminus	No-2							**-4777m** and **-1.0 km^2**
a		554	1889	30.2590	90.3711	51.5839	46.9910	
b		584	1904	30.2539	90.3796	51.2663	47.7999	
c		568	1918	30.2509	90.3739	50.9368	47.2480	
d		540	1902	30.2564	90.3661	51.5655	46.5094	

[2] These abbreviations will be used in tables 1-8.

Section of the topographic map in 1977

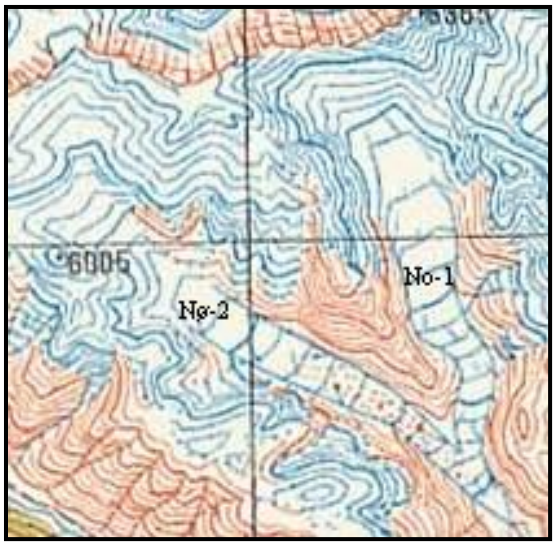

Map 3-1: Glacial tongues No-1 and No-2. Original terminus (black point); elevation 5250m.

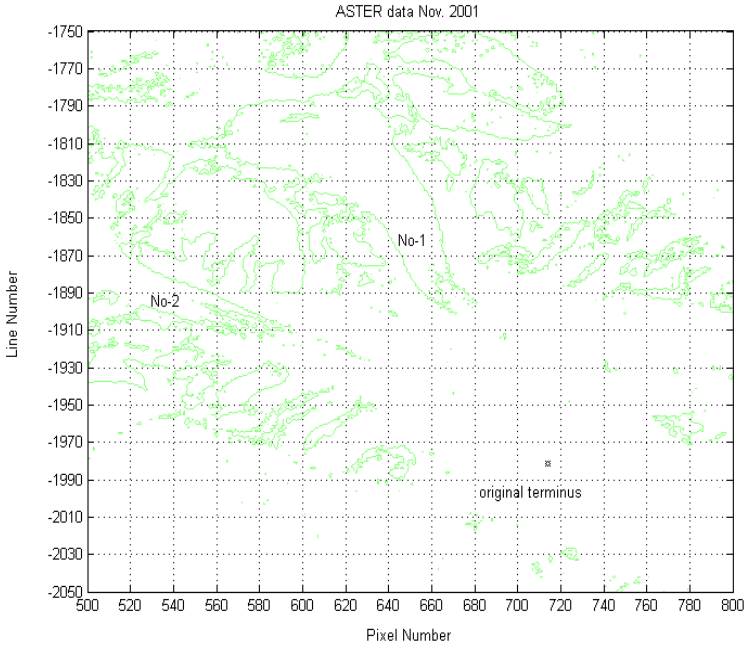

Fig 3-4: Glacial tongues No-1 and No-2, present termini; elevations 5730m and 5690m, respectively. Note the point of the original terminus.

Table 3-2: Comparison of original and present termini positions for tongues No-3 and No-4. Distance of receding calculated.

	Outlet number	IX	IY	Latitude	Longitude	Geo-north	Geo-east	Receding value
Original terminus	No-3							
a		1436	1295	30.3787	90.6727	64.4900	76.2900	
b		1435	1292	30.3795	90.6729	64.6000	76.2900	
c		1438	1291	30.3796	90.6738	64.6000	76.4000	
d		1439	1294	30.3785	90.6739	64.4900	76.4000	**-7833m** and **-7.1 km^2**
Present terminus								
a		1146	1275	30.3969	90.5848	66.7069	67.8795	
b		1162	1238	30.4050	90.5915	67.6843	68.5547	
c		1209	1267	30.3973	90.6046	66.5931	69.7884	
d		1188	1302	30.3878	90.5963	65.6732	68.9709	
Original terminus	No-4							
a		1034	1429	30.3614	90.5421	62.8500	63.7000	
b		1033	1415	30.3641	90.5420	63.1500	63.7000	
c		1043	1417	30.3642	90.5524	63.1500	64.0000	
d		1044	1427	30.3613	90.5390	62.8500	64.0000	**-939m** and **-1.4 km^2**
Present terminus								
		1023	1407	30.3670	90.5399	63.4812	63.5005	
		1000	1415	30.3659	90.5323	63.3722	62.7753	
		973	1384	30.3754	90.5260	64.4349	62.1798	
		997	1376	30.3780	90.5268	64.7256	62.2655	

Section of the topographic map in 1977

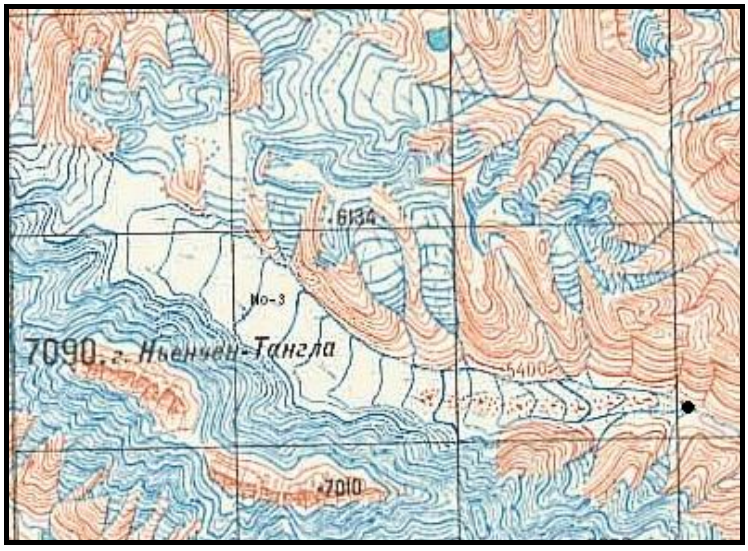

Map 3-2: Glacial tongue No-3, length 13660 m from terminus to root. Original terminus (black point); elevation 6090m.

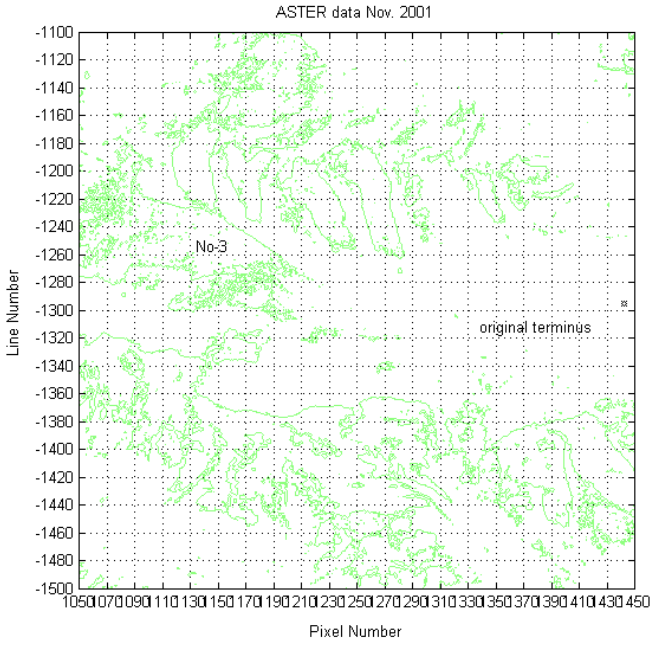

Fig 3-5: Glacial tongue No-3, present terminus position; elevation 6570m. 7830m from original position. Note the point of original terminus

.

Section of the topographic map in 1977

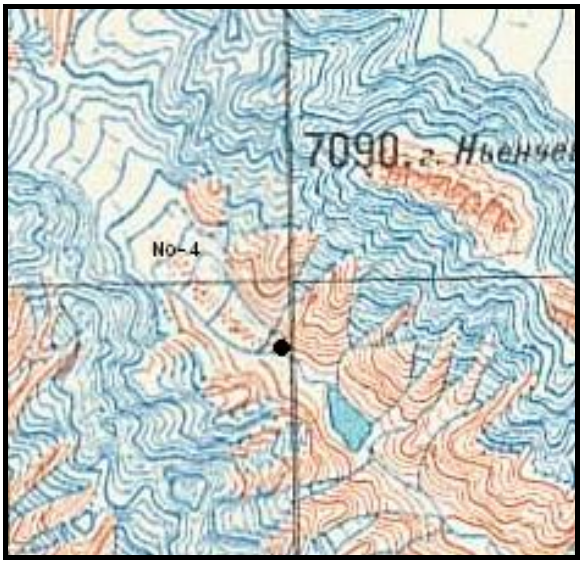

Map 3-3: Glacial tongue No-4, original terminus position; elevation 5440m.

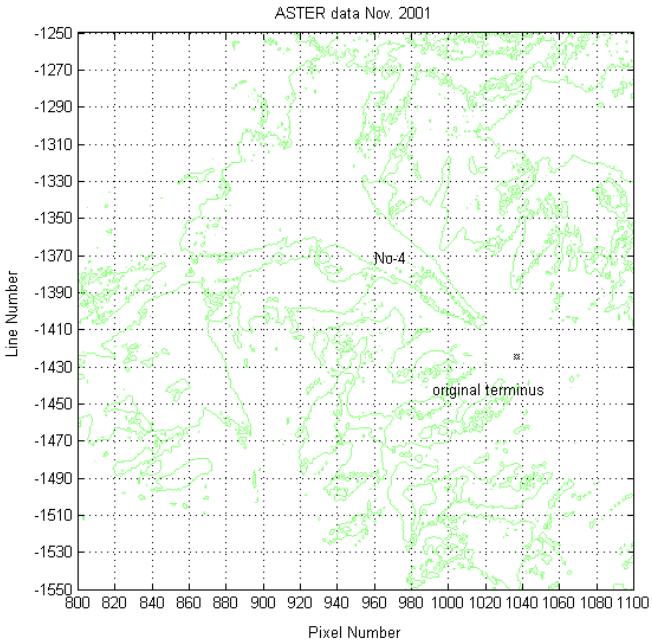

Fig 3-6: Glacial tongue No-4, present terminus position; elevation 5540m.
Note the point of original terminus.

Table 3-3: Comparison of original and present termini positions for tongues No-5 and No-6. Distance and area of receding calculated.

	Outlet number	IX	IY	Latitude	Longitude	Geo-north	Geo-east	Receding values
Original terminus	No-5							
a		1668	1143	30.4095	90.7522	67.7700	84.0000	
b		1663	1113	30.4175	90.7520	68.6500	84.0000	
c		1696	1108	30.4177	90.7624	68.6500	85.0000	
d		1701	1136	30.4097	90.7626	67.7700	85.0000	
Present terminus								**-516m**
a		1671	1100	30.4201	90.7554	68.9358	84.3287	and
b		1659	1118	30.4158	90.7508	68.4700	83.8728	**1.9 km^2**
c		1628	1100	30.4221	90.7421	69.1771	83.0565	
d		1640	1086	30.4252	90.7465	69.5244	83.4899	
Original terminus	No-6							
a		1640	1171	30.4033	90.7420	67.1000	83.0000	
b		1635	1141	30.4114	90.7418	68.0000	83.0000	
c		1667	1135	30.4116	90.7522	68.0000	84.0000	
d		1672	1165	30.4035	90.7524	67.1000	84.0000	**-616m**
Present terminus								and
		1639	1158	30.4060	90.7424	67.3975	83.0570	**0.7 km^2**
		1606	1132	30.4144	90.7336	68.3527	82.2262	
		1613	1100	30.4227	90.7374	69.2612	82.6127	
		1646	1128	30.4137	90.7462	68.2468	83.4322	

Table 3-4: Comparison of original and present termini positions for tongue No-7 distance of receding calculated.

	Outlet number	IX	IY	Latitude	Longitude	Geo-north	Geo-east	Receding value
Original terminus	No-7							
a		1594	1250	30.3840	90.7237	65.0000	81.2000	
b		1591	1233	30.3886	90.7236	65.5000	81.2000	
c		1609	1230	30.3887	90.7293	65.5000	81.7500	
d		1612	1246	30.3841	90.7294	65.0000	81.7500	**-2136m** and **-1.0 km^2**
Present terminus								
a		1550	1212	30.3955	90.7122	66.2975	80.1211	
b		1530	1202	30.3991	90.7065	66.7059	79.5854	
c		1530	1150	30.4131	90.7092	68.2461	79.8769	
d		1550	1160	30.4095	90.7149	67.8376	80.4125	

Section of the topographic map in 1977

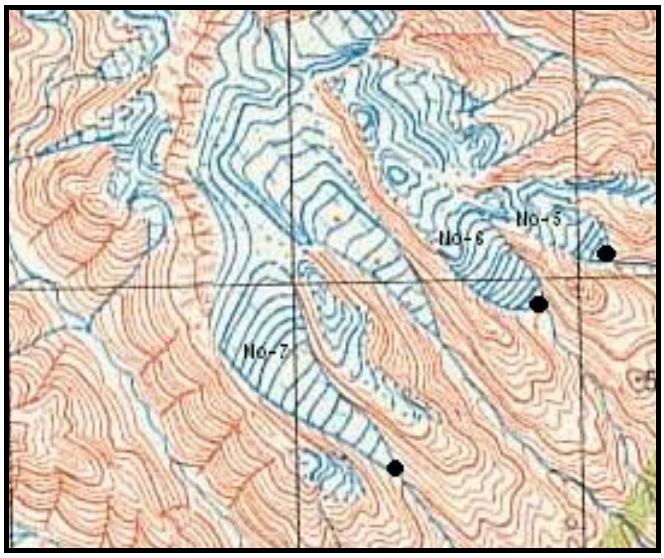

Map 3-4: Glacial tongues No-5, No-6 and No-7. Original termini (black point); elevations 5440, 5400m and 5200m respectively.

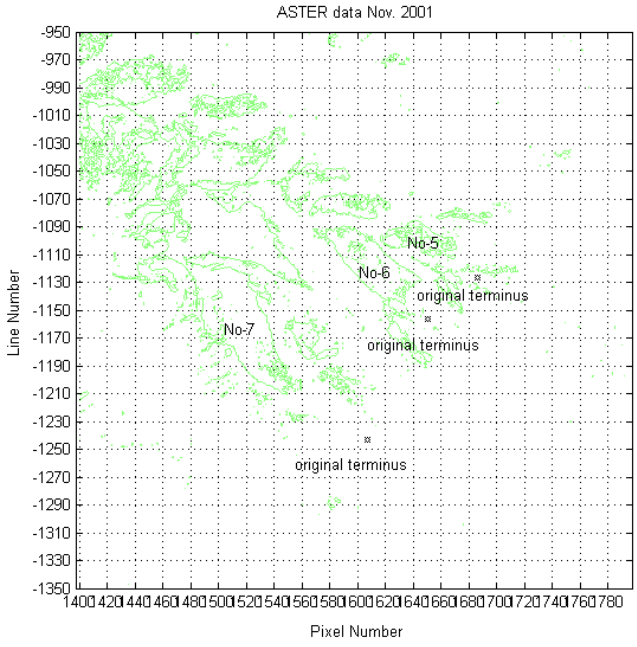

Fig 3-7: Glacial tongues No-5, No-6 and No-7, present termini; elevations 5640m, 5720m and 5480m, respectively. Note the point of original terminus

Table 3-5: Comparison of original and present termini positions for tongues No-8 and No-15. Distance of receding calculated.

	Outlet number	IX	IY	Latitude	Longitude	Geo-north	Geo-east	Receding value
Original terminus	No-8							
a		886	1540	30.3384	90.49078	60.4000	58.7000	
b		881	1514	30.3456	90.4905	61.2000	58.7000	
c		913	1508	30.3458	90.5009	61.2000	59.7000	
d		918	1534	30.3386	90.5011	60.4000	59.7000	
Present terminus								**-1854m**
a		884	1468	30.4568	90.4941	62.4397	59.0754	and
b		893	1462	30.3580	90.4972	62.5676	59.3753	**-0.6 km^2**
c		885	1447	30.3624	90.4955	63.0564	59.2228	
d		877	1452	30.3614	90.4927	62.9527	58.9581	
Original terminus	No-15							
a		1183	1264	30.3989	90.5963	66.9000	69.0000	
b		1162	1249	30.4038	90.5905	67.4500	68.4500	
c		1177	1230	30.4079	90.5961	67.9000	69.0000	
d		1196	1242	30.4039	90.6014	67.4500	69.5000	**-380m**
Present terminus								and
a		1190	1232	30.4062	90.6005	67.7061	69.4168	**-0.2 km^2**
b		1173	1232	30.4070	90.5952	67.8008	68.9138	
c		1173	1212	30.4124	90.5962	68.3932	69.0260	
d		1190	1212	30.4116	90.6015	68.2985	69.5290	

Section of the topographic map in 1977

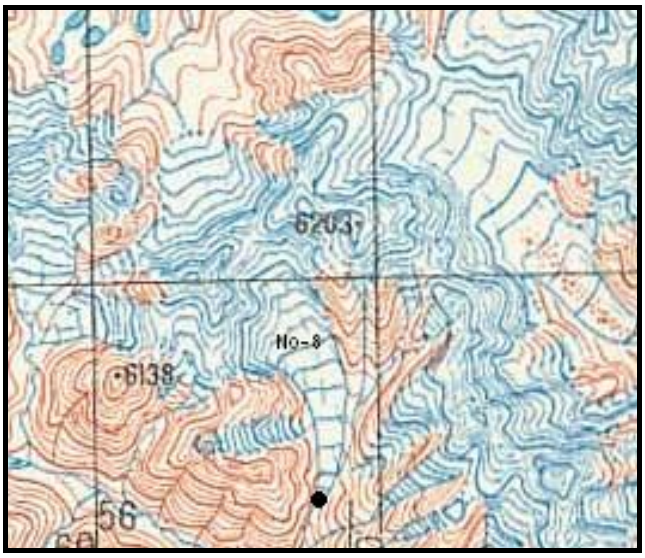

Map 3-5: Glacial tongue No-8. Original terminus (black point); elevation 5480 m.

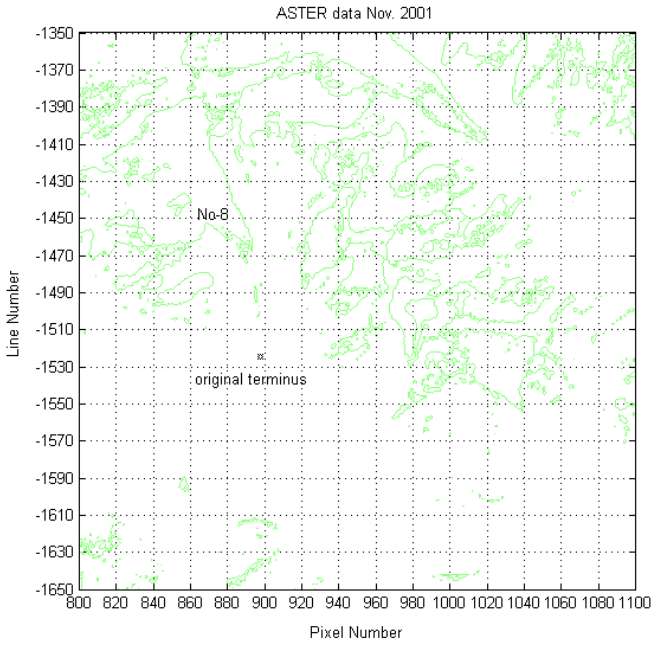

Fig 3-8: Glacial tongue No-8, present terminus; elevation 5720m. Note the point of the original terminus.

.

Table 3-6: Comparison of original and present termini positions for tongues No-9 and No-14. Distance of receding calculated.

	Outlet number	IX	IY	Latitude	Longitude	Geo-north	Geo-east	Receding value
Original terminus	No-9							
a		749	1549	30.4321	90.4475	60.9000	54.5500	
b		740	1512	30.3525	90.4472	62.0500	54.5500	
c		773	1505	30.3537	90.4576	62.2500	55.5500	
d		780	1543	30.3423	90.4579	60.9000	55.5500	**-4412m** and **-3.3 km^2**
Present terminus								
a		624	1644	30.3214	90.4052	58.6880	50.4312	
b		612	1626	30.3268	90.4024	59.2877	50.1772	
c		636	1614	30.3289	90.4104	59.5169	50.9546	
d		648	1632	30.3236	90.4131	58.9110	51.2086	
Original terminus	No-14							
a		1284	1143	30.4266	90.6336	69.9000	72.6500	
b		1267	1129	30.4310	90.6288	70.4000	72.2000	
c		1278	1111	30.4356	90.6334	70.9000	72.6500	**-1896m** and **-0.8 km^2**
d		1299	1124	30.4312	90.6392	70.4000	73.2000	
Present terminus								
a		1213	1156	30.4255	90.6115	69.8293	70.5234	
b		1172	1147	30.4298	90.5993	70.3244	69.3608	
c		1179	1104	30.4410	90.6037	71.5591	69.8085	
d		1219	1113	30.4368	90.6156	71.0697	70.9419	

Section of the topographic map in 1977

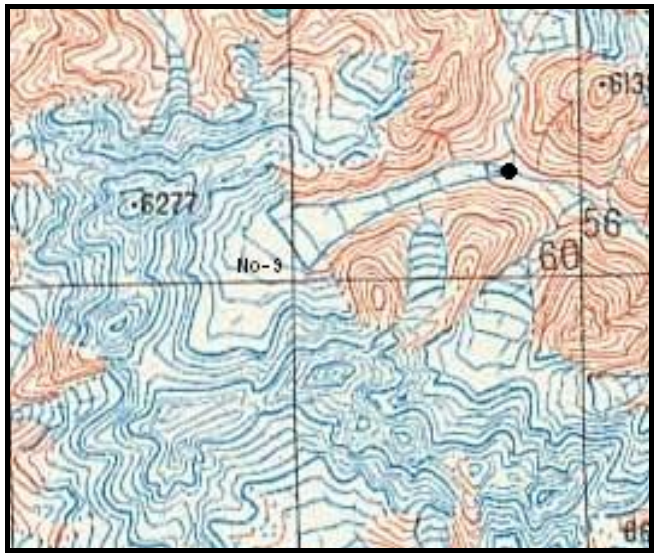

Map 3-6: Glacial tongue No-9. Original terminus (black point); elevation 5520 m.

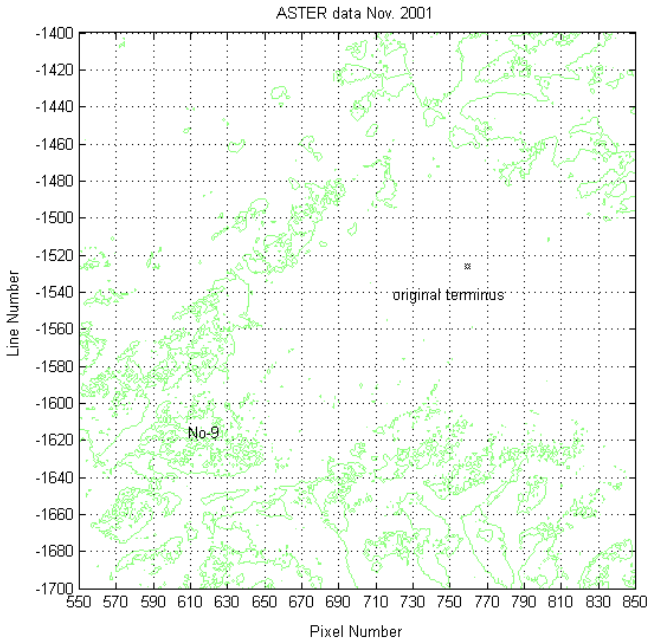

Fig 3-9: Glacial tongue No-9, present terminus; elevation 5960m. Note the point of the original terminus.

Section of the topographic map in 1977

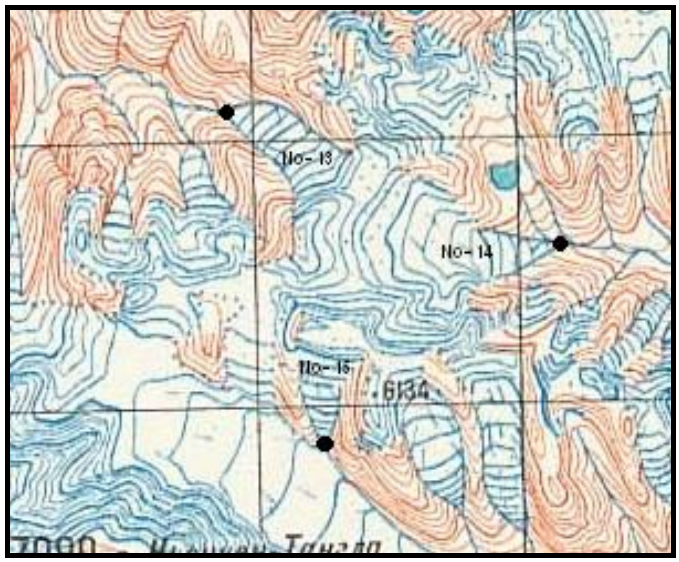

Map 3-7: Glacial tongues No-13, No-14 and No-15. Original termini (black point); elevations 5690m, 5890m and 5890m respectively.

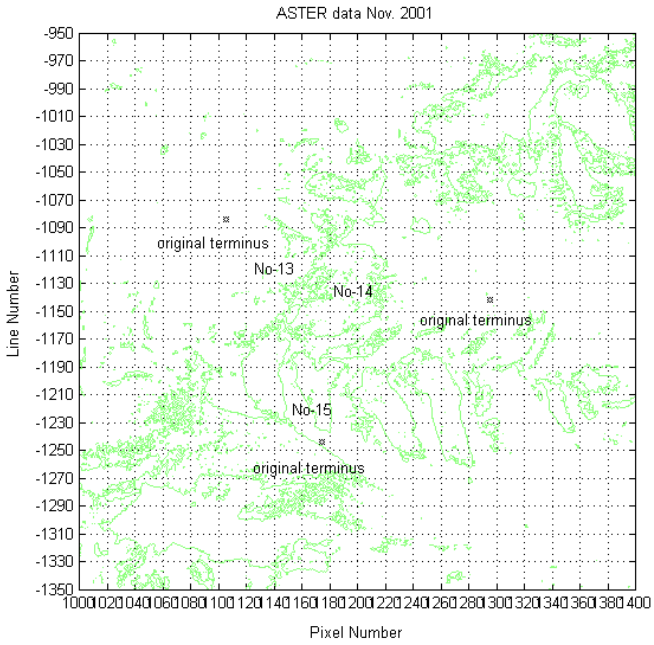

Fig 3-10: Glacial tongues No-13, No-14 and No-15, present termini; elevations 6290 m, 6170 m and 5970 m respectively. Note the point of the original termini.

Table 3-7: Comparison of original and present termini positions for tongues No-10 and No-13. Distance of receding calculated.

	Outlet number	IX	IY	Latitude	Longitude	Geo-north	Geo-east	Receding value
Original terminus	No-10							
a		307	1696	30.3224	90.3050	59.0000	40.8000	
b		300	1659	30.3324	90.3046	60.1000	40.8000	
c		333	1653	30.3325	90.3151	60.1000	41.8000	
d		340	1690	30.3226	90.3153	59.0000	41.8000	**-3135m** and **-1.6 km^2**
Present terminus								
a		406	1786	30.2932	90.3310	55.7060	43.2202	
b		381	1769	30.2988	90.3240	56.3474	42.5759	
c		391	1747	30.3043	90.3283	56.9443	42.9952	
d		415	1763	30.2989	90.3349	56.3381	43.6155	
Original terminus	No-13							
a		1107	1109	30.4437	90.5806	71.9000	67.6000	
b		1086	1092	30.4490	90.5753	72.5000	67.1000	
c		1100	1073	30.4536	90.5804	73.0000	67.6000	
d		1119	1086	30.4492	90.5857	72.5000	68.1000	
Present terminus								**-2047m** and **-2.2 km^2**
a		1170	1112	30.4393	90.6005	71|.3723	69.4977	
b		1148	1142	30.4322	90.5921	70.6061	68.6787	
c		1180	1168	30.4238	90.6007	69.6577	69.4797	
d		1197	1136	30.4316	90.6076	70.5109	70.1621	

Section of the topographic map in 1977

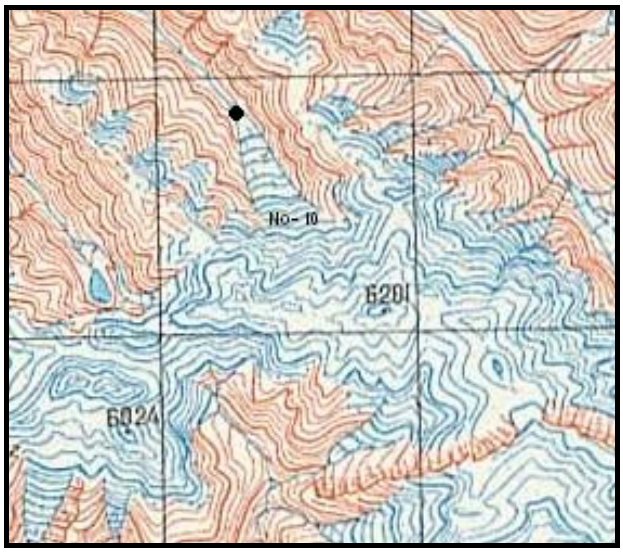

Map 3-8: Glacial tongue No-10. Original terminus (black point); elevation 5400 m.

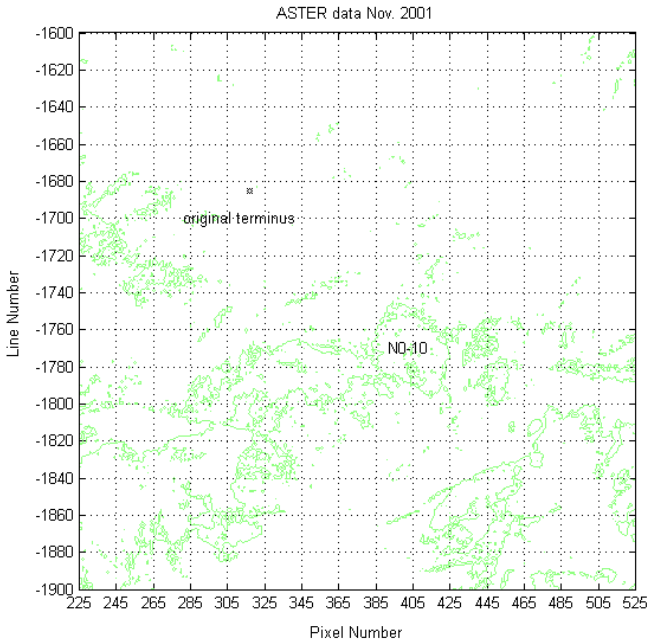

Fig 3-11: Glacial tongue No-10, present terminus; elevation 6040m. Note the point of the original terminus.

Table 3-8: Comparison of original and present termini positions for tongues No-11 and No-12. Distance of receding calculated.

	Outlet number	IX	IY	Latitude	Longitude	Geo-north	Geo-east	Receding value
Original terminus	No-11							
a		794	1377	30.3858	90.4707	65.7000	56.9000	
b		788	1345	30.3948	90.4705	66.7000	56.9000	
c		821	1338	30.3950	90.4809	66.7000	57.9000	
d		827	1371	30.3860	90.4811	65.7000	57.9000	**-794m** and **-0.9 km^2**
Present terminus								
a		800	1409	30.3763	90.4712	64.6537	56.9212	
b		795	1383	30.3835	90.4709	65.4518	56.9192	
c		828	1375	30.3842	90.4816	65.5058	57.9403	
d		832	1402	30.3768	90.4814	64.6836	57.9072	
Original terminus	No-12							
a		579	1511	30.3597	90.3976	62.9500	49.8000	
b		572	1477	30.3691	90.3973	64.0000	49.8000	
c		605	1471	30.3693	90.4077	64.0000	50.8000	
d		611	1505	30.3599	90.4080	62.9500	50.8000	
Present terminus								**-2707m** and **-1.8 km^2**
a		595	1595	30.3358	90.3987	60.3001	49.8482	
b		595	1567	30.3433	90.4001	61.1299	50.0053	
c		620	1567	30.3422	90.4078	60.9917	50.7449	
d		620	1595	30.3347	90.4064	60.1620	50.5878	

Section of the topographic map in 1977

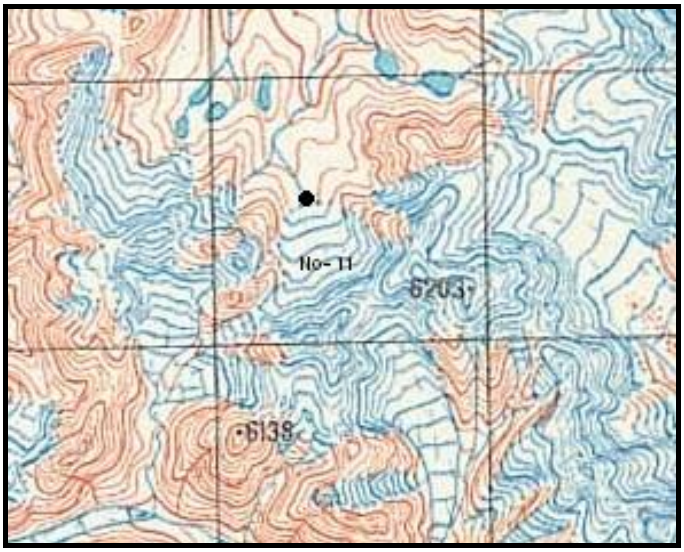

Map 3-9: Glacial tongue No-11. Original terminus (black point); elevation 5680m.

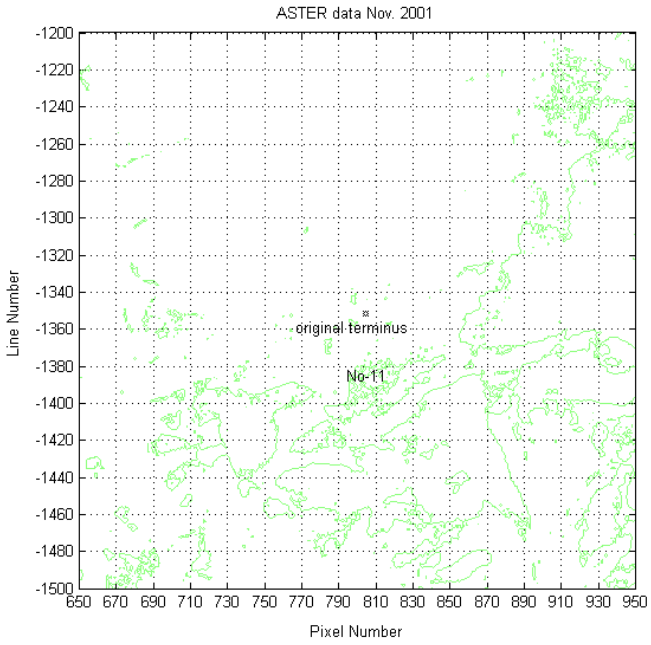

Fig 3-12: Glacial tongue No-11, present terminus; elevation 5800m. Note the point of the original terminus.

Section of the topographic map in 1977

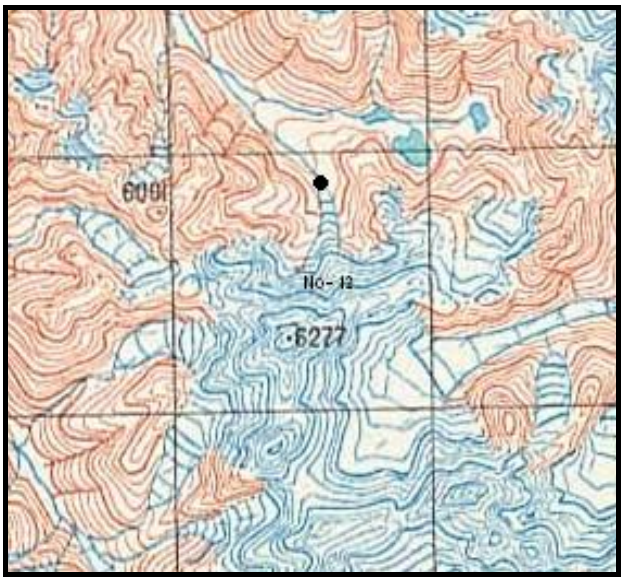

Map 3-10: Glacial tongue No-12. Original terminus (black point); elevation 5640 m.

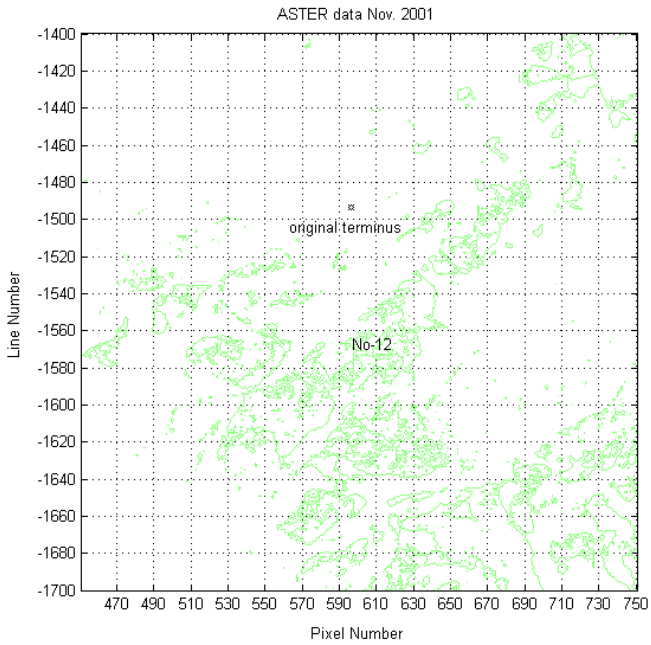

Fig 3-13: Glacial No-12, present terminus; elevation 6280 m. Note the point of the original terminus.

3.3 Different phenomena and the extent of retreat between the north-western and south-eastern parts of the NyainQen TangLha glacier.

The 1977 topographical map shows that there were only a few small glacial tongues on the north-western part of the NyainQen TangLha glacier whereas there were many, much larger glacial tongues on the south-eastern part of the glacier.

The ASTER data shows an overall retreat of the whole glacier and the glacial tongues on the southern part which have retreated much more than those on the northern part of the glacier. The data substantiating this is collected and listed in Table 3-9.

Three elevations have been calculated; (1) elevation at the top of the glacier in 1977 (H). (2) elevation of glacial termini in 1977 (H_1) (3) elevation of glacial termini in 2001 (H_2). The difference in elevation of glacier termini between 1977 and 2001 is $\Delta H = H_2 - H_1$.

Two lengths have been calculated; (1) the original length of the glacial tongue, from the head of the tongue to its termini (L), (2) the distance between of the termini of 1977(**A**) and 2001(**B**) is ΔL and is calculated from topographical and ASTER data.

The slope angle a is estimated from ΔH, and ΔL; $\tan a = \frac{\Delta H}{\Delta L}$ (see Fig 3-14). The change was calculated in the positions of the termini from their original positions to their present. The percentage that the change represented was then calculated by taking the change in terminus position (ΔH) and dividing it by the original length of glacial tongue (L).

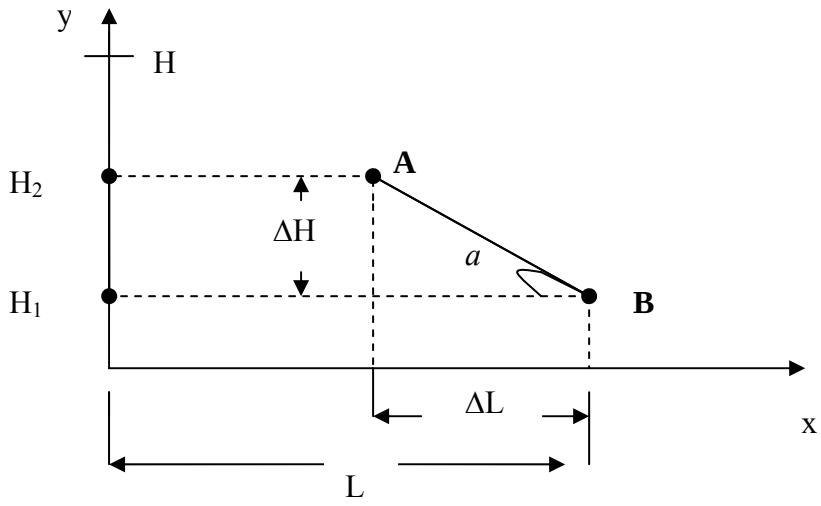

Fig 3-14: The determination of slope angle.

Table 3-9: Summary of data on position of glacial tongues in 1977 and 2001 NyainQen TangLha glacier. The percentage of receding and concomitant conditions of the two sides of the glacier.

TN[1]	EOGT[2] H (m)	Elevation of original terminus H_1 (m)	Elevation of present terminus H_2 (m)	Slope angler *a*	FO[3]	TOGT[4] L (m)	DOR[5] ΔL (m)	PR[6] %
No-1	6370	5250	5690	8.5°	NW-SE	6180	2930	47
No-2	6010	5250	5730	5.7°	NW-SE	6390	4780	75
No-3	6850	6090	6570	3.5°	NW-SE	11310	7830	69
No-4	6160	5440	5540	3.4°	NW-SE	3370	1670	50
No-5	6000	5440	5640	21.2°	NW-SE	2040	520	25
No-6	6000	5400	5720	27.5°	NW-SE	2800	620	22
No-7	6000	5200	5480	7.5°	NW-SE	3880	2140	55
No-8	6040	5480	5720	7.4°	N-S	2870	1850	65
No-15	6970	5860	5970	17.4°	N-S	1650	380	23
No-9	6280	5520	5960	5.7°	W-E	4470	4410	99
No-14	6970	5890	6170	8.4°	W-E	1990	1990	100
No-10	6200	5400	6040	11.5°	SE-NW	3140	3140	100
No-13	6970	5890	6290	11.1°	SE-NW	2050	2050	100
No-11	6040	5680	5800	8.6°	S-N	860	790	92
No-12	6280	5640	6280	13.3°	S-N	2710	2710	100

[1] Tongue number [2]Elevation of glacial top [3]Flowing orientation [4]Total length of glacial tongue

[5]Distance of receding [6]Percentage of receding

Chapter 4

Discussion

4.1 Summary of chapter three

The results of the previous chapter will be discussed:

(1) It was observed that the position of the glacial tongues of all the fifteen glaciers that have been studied had retreated during the last 24 years.

(2) A marked difference was found in the retreat of the glacier tongues on the two sides of the glacier.

4.2 Processes resulting in changes of the position of the glacial tongue

If the rate of accumulation in winter is greater than the melting of snow and ice during the ablation season, snow will start to accumulate. When this situation occurs over many years, the snow/ice volume will become so vast that the ice mass will start to deform due to the gravity. The ice masses will start to move. Thus a snow field has been transformed to a glacier. If the mass balance is positive, the tongue of the glacier will move down the valley. On the other hand, if the accumulation in winter decreases and/or the rate of melting in summer increases, the volume of the glacial tongues decrease and the position of the glacial tongues may retreat. The glacier will respond to climatic change; however the relationship between the position of the glacier tongue and climatic change may be masked. The change in the position of the glacial tongues can be a result of**:**

A. Change in ablation

B. Change in accumulation

In this section an attempt will be made to determine and then discuss the reasons for the negative long term mass balance found in all the test-sites in relation to climactic factors: temperature and precipitation. Climate change is considered to be a key function which affects of mass balance of glacier changes. Though short term climate change has no substantial affect on a glacial tongue's advance and recession, long term climate system change on the other hand does have a significant influence on a glacial tongue's advance and recession (Dyurgerov, 1997).

The relationship between glacial fluctuations of the position of glacial tongues and climatic change is complex and are involving processes that are not fully understood. Change in accumulation is related to changes in the annual precipitation and length of the accumulation seasons which in turn is related to air temperature. Change in accumulation could also be result of a change in wind patterns.

Change of ablation is related to changes in air temperature and wind, cloud cover and surface albedo.

While mass input is largely from snowfall or winter precipitation, mass output is controlled by the energy fluxes to or from a glacier. In general, total energy is influenced by short-wave and long-wave radiation, sensible heat, and latent heat transferred by phase change. Based on these concepts, loss in glacial mass and retreat of glacial tongues may intuitively take place during periods of increased annual and seasonal air temperature, which may be accompanied by decreased snow precipitation.

4.2.1 Ablation and accumulation season

4.2.1.1 Ablation season

Monthly mean air temperature and precipitation record from Lhasa station (30°N, 90°10'E, 3760 m a.s.l.) that were obtained from the Global Historical Climatology Network[3] (Peterson 1997) during 1950-1990. (Table 4-1).

Table 4-1: Monthly mean air temperature in Lhasa station (3760m a.s.l).

Month	J	F	M	A	M	J	J	A	S	O	N	D
Mean air temperature (°C)	- 1.4	+ 1.4	+ 4.7	+ 8.7	+ 12.8	+ 16.3	+ 16.3	+ 15.5	+ 10.9	+ 9.2	+ 3.4	- 0.5

[3] It is a comprehensive glob surface climate data set designed to be used to monitor and detect climate change in Bergen (60.4°N, 5.3°E; 45 m a.s.l.).

Table 3-9 showed that the mean elevation of the fifteen glacial tongues is 5575m. The mean altitude difference between Lhasa and the fifteen glacial tongues is 1815m. The rough monthly mean air temperature of the fifteen glacial tongues can be calculated by the *lapse rate.*

$$T_G = T_L - \gamma \Delta Z$$

Where T_G and T_L stand for the monthly mean air temperature of the fifteen glacial tongues and Lhasa, respectively. γ =0.65°C/100m which is assumed to be the mean temperature gradient in the lowest part of the atmosphere and ΔZ is the altitude difference between Lhasa and the fifteen glacial tongues. So the temperature difference between the two areas can be calculated to 11.8°C. Table 4-2 shows the rough monthly mean air temperature estimated for the fifteen glacial tongues:

Table 4-2: Rough monthly mean air temperature of the fifteen glacial tongues (5575 m a.s.l).

Month	J	F	M	A	M	J	J	A	S	O	N	D
Mean air temperature (°C)	- 13.2	- 10.3	- 7.1	- 3.1	+ 1.0	+ 4.5	+ 4.5	+ 3.7	- 0.9	- 2.6	- 8.4	- 11.3

The transition between air and sleet is normally at about 1°C. However, this will vary with the temperature gradient in the, say, lowest 100 m above the surface. Here we will use $T_G \leq$ 0°C for snow and T_G >0°C for rain. So Table 4-2 shows the ablation season should be May, June, July and August, and the mean air temperature for this season is 3.4°C

Assuming a 1°C increase in air temperatures in both ablation and accumulation seasons Fig 4-1 shows the relationship between temperature and total days in both ablation and accumulation seasons. The approximate length of the ablation season with an average temperature of 3°C is 120 days.

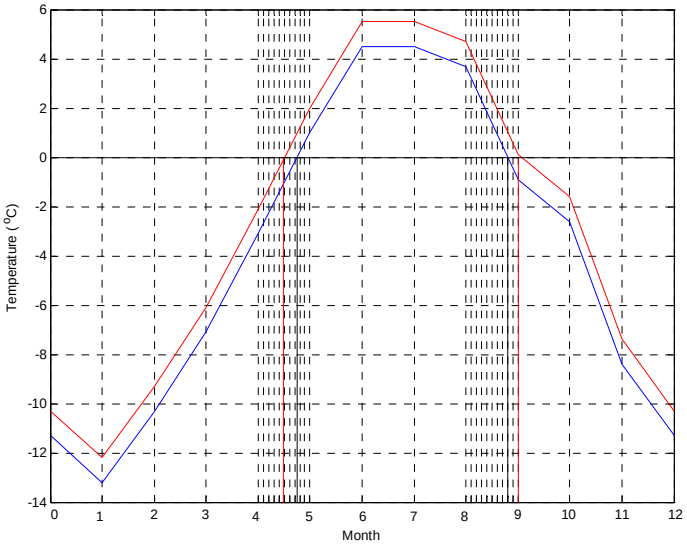

Fig 4-1: An increase in mean seasonal air temperature of 1°C in ablation and accumulation, respectively. This would lead to an increase in ablation of 16 days. The length between the blue and red line is day difference in ablation season.

4.2.1.2 Accumulation season

From Table 4-2 and Fig 4-1 show that the mean monthly temperature is -7°C during the accumulation season which lasts for 245 days. A 1°C increase in air temperature would lead to a shortening of the accumulation season by 16 days. In Addition Table 4-3 shows mean monthly precipitation in Lhasa.

Table 4-3: Mean monthly precipitation in Lhasa station.

Month	J	F	M	A	M	J	J	A	S	O	N	D
Precipitation (mm)	0.4	0.6	2.1	6.2	24	77	128	135	57	8.9	1.3	0.7

According to Table 4-3, the mean precipitation in the accumulation and ablation season can be calculated to 9.7 mm and 91mm, respectively. Mean monthly precipitation is 36.7 mm. If we assume that Lhasa and NyainQen TangLha Glacier has the same variation of precipitation during the years, we see from the table that 15-20% of the precipitation is snow.

4.2.2 Calculation of ablation

The heat used for ablation can be expressed by following equation (Paterson 1994):

$$M + \Delta G = R + Q_H + Q_E + L_f P' \quad (Wm^{-2}) \tag{4.1}$$

$$Q_E = -E\,Lv \tag{4.2}$$

Here:

M = heat used to melt snow and ice. If melt-water refreezes in the snow pack, this term represents a gain in heat; it is then negative.

ΔG = rate of gain of heat of a vertical column from the surface to the depth at which vertical heat transfer is negligible.

R = net radiation,

Q_H = sensible heat flux. If the surface is warmer than the air, Q_H is negative.

Q_E = latent heat flux.

Lv = specific latent heat of vaporization ($2.8 \cdot 10^6$ J k g^{-1}).

E = rate of evaporation from surface, if water-vapour pressure decreases with height. If there is condensation on the surface, E is negative. Turbulence increases the rate of transfer of water vapour between the atmosphere and the surface.

L_f = specific latent heat of fusion of ice ($3.34 \cdot 10^5$ J k g^{-1}).

P' = precipitation rate of rain. The heat supplied by rain is negligible when the surface is melting but may be significant if the rain can freeze. S.I.[4] units for each term Eq (4.1) are Wm^{-2}.

The net radiation is

$$R = Q\,(1-\alpha) + L^{\downarrow} + L^{\uparrow} \tag{4.3}$$

Here:

Q = rate of incoming solar radiation (direct and scattered) at the surface.

α = surface albedo (ratio of reflected to incidence solar radiation).

$L^{\downarrow}$ = rate of incoming long-wave at the surface.

$L^{\uparrow}$ = rate of emission of long-wave radiation by the surface.

[4]I.S. stands for international system of units.

The most important terms in Eq (4.1) are sensible heat flux Q_H, latent heat flux Q_E and net radiation R.

There are no meteorological data available from the NyainQen TangLha area. The different terms in Eq (4.1) can therefore not be determined based on data from the district.
Relevant data would be air temperature, air humidity, wind speed, albedo of glacier surface and cloud cover.

4.2.2.1 Sensible and latent heat flux

Both the sensible and the latent heat fluxes are related to air temperature and wind speed. We can see that both air temperature and wind speed play a significant role in the ablation.

(1) The relationship between sensible heat flux and air temperature, and wind speed can be expressed:

$$Q_H = \rho c_p k_h \frac{\partial T}{\partial z} \ (\mathrm{Wm^{-2}}) \qquad (4.4)$$

Here ρ is the density of air, c_p its specific heat capacity at constant pressure, k_h is eddy diffusivity and T is air temperature at height z. In the atmosphere; Molecular conduction is insignificant compared with convection and k_h is order of magnitude of 10^5 times the molecular thermal diffusivity. The coefficient k_h is a function of z, u, $\frac{\partial T}{\partial z}$ and z_0 etc. If its value is known, then Q_H can be calculated from measurements of T at different heights. The transfer of heat and water vapour by convection depends on the turbulence of the air. This is measured by the eddy viscosity k_m defined by the equation (Paterson 1994):

$$\tau = \rho k_m \frac{\partial u}{\partial z} = \rho u_*^2 \qquad (4.5)$$

Here τ is the shear-stress in the air above the surface; u is the wind speed at height z and u_* is the friction velocity. Experiments show that the shear stress τ variation with height is

small and a reasonable approximation is (Paterson 1994): $\frac{\partial \tau}{\partial z} = 0$ in the *constant flux layer* 0-50m above the surface: For neutral or near neutral stratification it can be shown that

$$k_m = u_* k_0 z. \tag{4.6}$$

Here k_0 is called *von Karman's constant* with a value of 0.4.

Eq (4.4) then shows that.

$$k_m \frac{\partial u}{\partial z} = \frac{\tau}{\rho} \equiv u_*^2 = \text{constant} \Rightarrow \frac{u}{u_*} = \frac{1}{k_0} \ln\left(\frac{z}{z_0}\right) \tag{4.7}$$

Here z_0 is the surface roughness parameter.

A simple relation is used to calculate the sensible heat flux.

From Eq (4.4) and (4.6) with $k_h = k_m$,

$$Q_H = c_P \rho k_0 u_* z \frac{\partial T}{\partial z} \, (\mathrm{Wm^{-2}}) \tag{4.8}$$

Integration gives

$$Q_H = c_P \rho k_0 u_* \frac{T - T_s}{\ln\left(\frac{z}{z_0}\right)} \, (\mathrm{Wm^{-2}}) \tag{4.9}$$

Here T_s is surface temperature. Substitution for u_* from Eq (4.7) gives

$$Q_H = c_P \rho k^2{}_0 u \frac{T - T_s}{\left[\ln\left(\frac{z}{z_0}\right)\right]^2} \, (\mathrm{Wm^{-2}}) \tag{4.10}$$

This can be written

$$Q_H = \rho \, c_P A u (T - T_s) \, (\mathrm{Wm^{-2}}) \tag{4.11}$$

Where

$$A = \frac{k_0^2}{\left[\ln\left(\frac{z}{z_0}\right)\right]^2}. \tag{4.12}$$

The dimensionless parameter *A* is called the transfer coefficient. If the height z =2m above the surface, and according to (Alt, 1975) for ice in ablation zone $z_0 = 10^{-3}$ m, then the dimensionless parameter *A* can be calculated to $2.8*10^{-3}$. The density of air is expressed by $\rho = \rho_0(\frac{P}{P_0})$, P is atmospheric pressure and ρ_0 the density at standard pressure P_0.

Substitution of numerical values $\rho_0 = 1.29 \mathrm{kg\,m^{-3}}$, $P_0 = 1.013 \cdot 10^5$ Pa, $c_P = 1010 \mathrm{\,Jkg^{-1}K^{-1}}$ gives

$$Q_H = (1.29 \cdot 10^{-2}) A \rho u (T - T_s) \ (\mathrm{Wm^{-2}}) \tag{4.13}$$

This equation is used to calculate the sensible heat available for ablation, in which case T_s =273 K.

It is difficult to estimate the wind condition in the region during the ablation seasons which also will shows large local variation. A rough estimate based on discussions with local people would be $3 \mathrm{m\,s^{-1}}$.

In addition, the relationship between air pressure and altitude can be written:

$$\frac{dP}{P_0} = -\frac{dz}{H_0} \Rightarrow P = P_0 e^{\frac{-z}{H_0}} \tag{4.14}$$

Here H_0 and P_0 are the scale height and mean global surface pressure of 1.01325 Mpa, respectively. For the mean temperature of Earth's atmosphere H_0 is about 7.6 km (Hartmann 1994). Fig 4-2 shows vertical distribution of the air pressure P as a function of altitude for globally and annually averaged conditions.

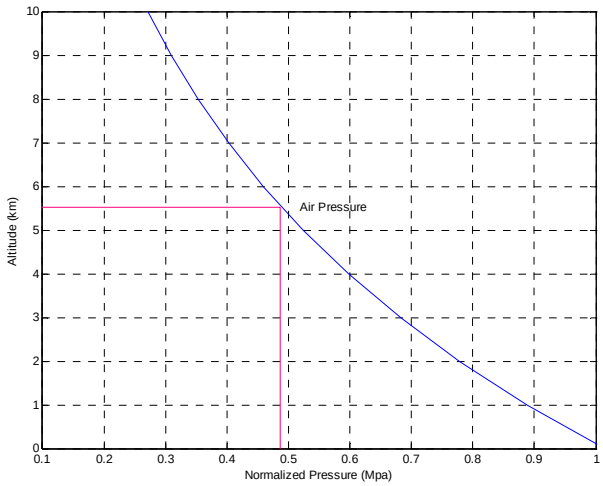

Fig 4-2: Vertical distribution of air pressure as a function of altitude (based on Eq (4.14)). The red line is air pressure of 5575 m, and is equal to $4.9 \cdot 10^4$ (Pa).

The energy flux of the ablation period expressed as energy flux Ψ ($J \cdot m^{-2}$).

For sensible heat flux:

$$\Psi = Q_H \Delta t \qquad (4.15)$$

Here Δt is the length of the ablation period.

Then $\Psi = 1.29 \cdot 10^{-2} \cdot 2.8 \cdot 10^{-3} \cdot 4.9 \cdot 10^4 \cdot 3 \cdot 3 \cdot 120 \cdot 24 \cdot 3600 = 1.7 \cdot 10^8$ (Jm^{-2}), Divided by specific latent heat of fusion of ice, $L_f = 3.34 \cdot 10^5$ ($J\,k\,g^{-1}$), gives $W = \Psi / L_f = 509$ ($kg\,m^{-2}$) equivalent to 509 mm of water. Here W is mass of melting water.

If we assume that the wind conditions are constant and the air temperature is increased by 1°C, the ablation season will consequently increase to a total of 136 days. Then Fig 4-3 shows a projection of the trend in the relationship between increased air temperature and mass of melting water. The heat comes from sensible heat flux.

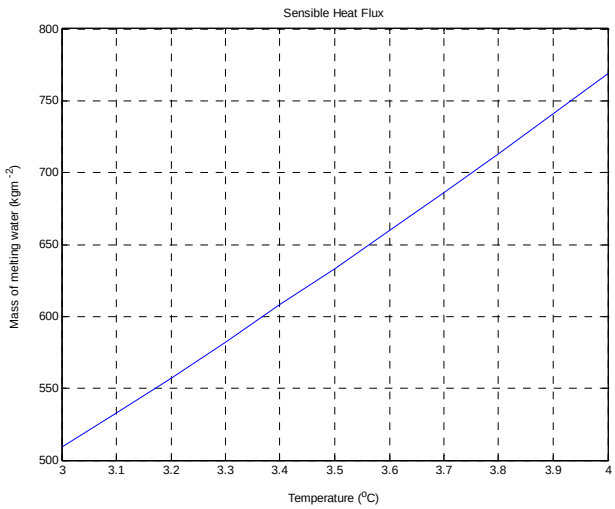

Fig 4-3: An increase in mean air temperature of 1°C in ablation season and a constant wind speed of 3m will lead to an increase in ablation of 253 $\mathrm{kg\,m^{-2}}$ equivalent to 253 mm of water.

If we assume that the air temperature is constant and the wind speed changes by 1m/s. Then Fig 4-4 shows a projection of trend in the relationship to the increased wind speed and the mass of melting water. The heat comes from sensible heat flux.

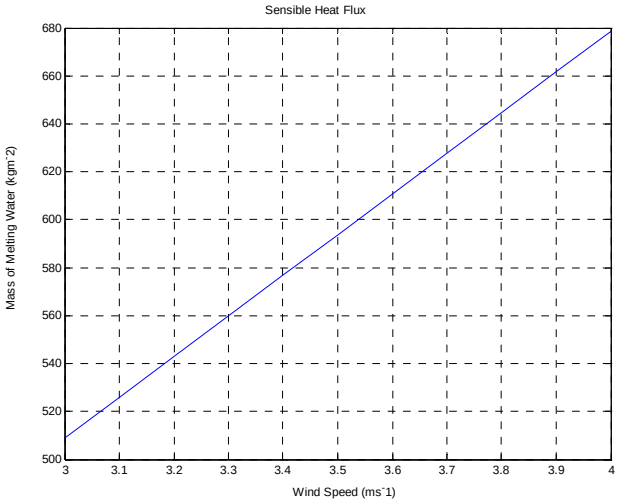

Fig 4-4: An increase of wind speed of 1$\mathrm{m\,s^{-1}}$ during the ablation season and constant mean air temperature of 3°C will lead to an increase in ablation of 170 $\mathrm{kg\,m^{-2}}$ equivalent to 170 mm of water.

(2) The relationship between latent heat flux and air temperature, and wind speed that can be expressed:

$$Q_E = -E\,Lv = -Lv\,k_w\left(\frac{0.622\rho}{P}\right)\frac{\partial e}{\partial z} \quad (\mathrm{Wm^{-2}}) \qquad (4.16)$$

In Eq (4.1) it was also shown that latent heat plays an important role in the process of snow and ice melting. The relationship between the latent heat and vapour pressure is given in Eq (4.16).

Where k_w is called the *eddy diffusivity* for water vapour. P is the atmospheric pressure, ρ is density of air and e is the pressure of the water vapour in the atmosphere at height *z*.

From Eq (4.16) and (4.7) and we assume that $k_w = k_m$,

$$Q_E = 22.2Au\,(e - e_s) = 6.2 \cdot 10^{-2}\,u\,(e - e_s) \quad (Wm^{-2}) \tag{4.17}$$

$$e = R_H e_s \,(Pa) \tag{4.18}$$

Where e and e_s is vapour pressure at height of 2m and at the surface, respectively. For a melting surface e_s = 611Pa. R_H is relative humidity, the mean R_H in Lhasa during ablation season is about 80% (MTAR[5], 1982). If we assume an air temperature of 3°C and a constant mixing ratio with height, lifting condensation level will normally be below the glacial area. Probably the best estimate of relative humidity in the glacial area is 100%. The vapour pressure e at a height of 2m can be expressed (Ahrens 1999):

$$e = R_H e_s\,(3°C) = 765\ (Pa) \tag{4.19}$$

And use Eq (4.15), then Eq (4.17) can be written:

$$\Psi = 6 \cdot 10^{-2} \cdot 120 \cdot 24 \cdot 3600u\,(765 - 611)\ (Jm^2)$$

The mass of melting water can then be calculated:

$$W = \frac{\Psi}{L_f} = = 860\ (kg\,m^{-2})$$ equivalent to 860 mm of water.

Assuming constant wind conditions and an increase in air temperature of 1°C, Fig 4-5 shows the relationship of increased air temperature and mass of melting water, consequently the ablation season changes to 136 days and e changes to 840 Pa. The heat comes from latent heat flux.

[5] Meteorology in Tibet Autonomous Region

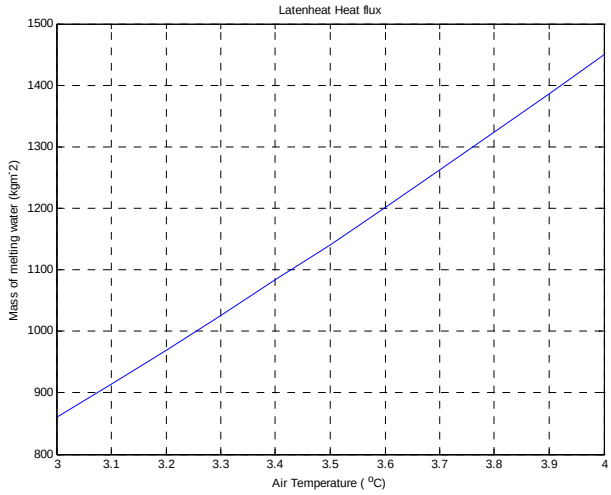

Fig 4-5: An increase in mean air temperature of 1°C in ablation season and a constant wind speed of 3 m/s will lead to an increase in ablation of 590 $\mathrm{kg\,m^{-2}}$ equivalent to 590 mm of water.

Assuming constant air temperature and an increase in wind speed of 1m/s, Fig 4-6 shows a projection in trend between increased wind speed and mass of melting water. The heat comes from latent heat flux.

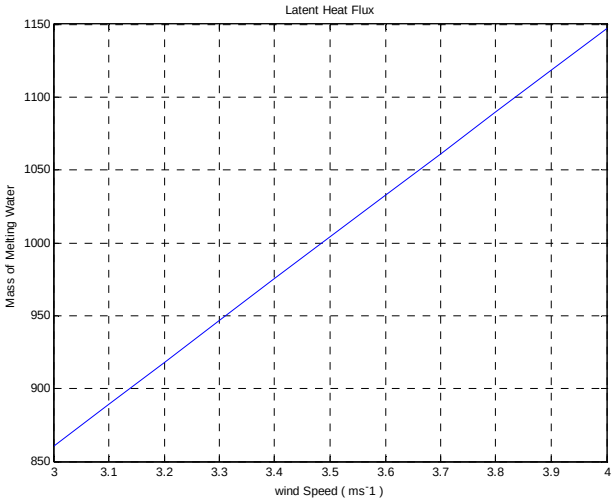

Fig 4-6: An increase of wind speed of 1 $\mathrm{m\,s^{-1}}$ during the ablation season and constant mean air temperature of 3°C will lead to an increase in ablation of 287 $\mathrm{kg\,m^{-2}}$ equivalent to 287 mm of water.

4.2.2.2 Radiation

Both the incoming long-wave and short-wave radiation is calculated with a theoretical cloudless condition. In the following they are calibrated by an index between nearly overcast and cloudless condition.

(1) Long-wave radiation

(A) The relationship between incoming long wave radiation and air temperature under the nearly cloudless condition can be expressed.

$$L^{\downarrow} = \varepsilon \sigma T^4 \ (Wm^{-2}) \tag{4.20}$$

Where T is air temperature 2m above surface (Olseth, 1996), σ is *Stefan'constant* which has a value of $5.67 \cdot 10^{-8}$ $W m^{-2} K^{-4}$.

$$\varepsilon = (\frac{T}{T_*})^2, \tag{4.21}$$

Where T_* is equal to 326.8 *K* (Czeplak and Kasten, 1987).

Combining Eq (4.19) and (4.20) give the following:

$$L^{\downarrow} = \sigma \frac{T^6}{T_*^2} (Wm^{-2}) \quad \Rightarrow \quad \Psi^{\downarrow} = 5.32 \cdot 10^{-13} \cdot 120 \cdot 24 \cdot 3600 \cdot 276^6 = 2.44 \cdot 10^9 \ (Jm^{-2}).$$

The ratio of long-wave irradiation between nearly overcast and nearly cloud-less condition is 1.2 (Olseth, 1993). Consequently, the mean long-wave irradiance, relative to the two conditions, can be calculated to $2.682 \cdot 10^9$ Jm^{-2}.

$$\Rightarrow W = \Psi^{\downarrow} / L_f = 8030 \ (kg\, m^{-2})$$

(B) the relationship between outgoing long-wave radiation and surface temperature can be expressed:

$$L^{\uparrow} = \sigma T_s^4 \ (Wm^{-2}). \tag{4.22}$$

Here T_s is surface temperature of the glacier of 0°C.

$\Psi^{\uparrow} = 5.67 \cdot 10^{-8} \cdot 273^4 \cdot 10368000 \ (Jm^{-2}) \Rightarrow W = \Psi^{\uparrow} / L_f = 9777 \ (kgm^{-2})$.

Consequently the mass of melting water resulting from the net long-wave radiation can be expressed:

$W_{L\text{-}W} = \Psi^{\downarrow} / L_f - \Psi^{\uparrow} / L_f = -1747 \ (kgm^{-2})$.

(2) Short wave radiation

The relationship between incoming short-wave radiation and albedo will be expressed:

$$S = Q\,(1-\alpha)\ (Wm^{-2}) \qquad (4.18)$$

Where S is net short wave radiation and Q is incoming short wave irradiance at the surface that is computed by *the global irradiance model* (Olseth, 1989). Fig 4-7 shows the monthly incoming short wave irradiance of the fifteen glacial tongues from May to August of which the albedo is estimated 0.7 and in clear sky. The mean monthly sum of incoming short-wave irradiance of the fifteen glacial tongues in ablation season is $9.84{\cdot}4{\cdot}10^{8}$ (Jm^{-2}).

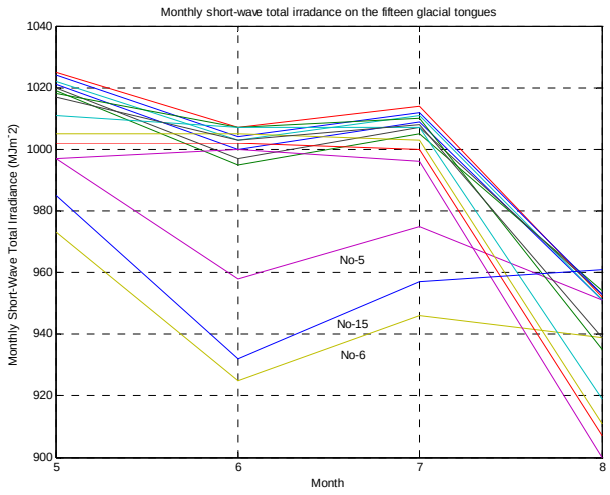

Fig 4-7: May to August monthly incoming short-wave irradiance of the fifteen glacial tongues.

The ratio of short-wave radiation between nearly overcast and nearly cloud-less conditions is 0.5 (Olseth, 1993). Consequently, the mean sum of short-wave radiation of 15 glacial tongues for the ablation season, relative to the two conditions, can be calculated as $2.95{\cdot}10^{9}$ Jm^{-2}.

And use Eq (4.15), then Eq (4.18) can be written:

$\Psi = 8.85{\cdot}10^{8}(\mathrm{J\,m^{-2}}) \Rightarrow W_{S\text{-}W} = \dfrac{\Psi}{L_f} = 2.65{\cdot}10^{3}\ (\mathrm{kg\,m^{-2}})$, equating to 2650 mm of water.

(3) Net radiation

The mass of melting water as a result of net radiation can be expressed:

$W_{net}=W_{S-W}+W_{L-W}=903$ (kgm^{-2}).

If we assume an increase in the mean air temperature of 1°C during the ablation season and hold both Q and α constant. It will lead to an increase in ablation due to increased incoming long-wave radiation of 1270 kgm^{-2}, due to outgoing long-wave radiation of 1303 kgm^{-2} and the incoming short-wave radiation of 355 kgm^{-2}. Then Fig 4-8 shows a projection of the trend between an increase in air temperature and mass of melting water. The heat comes from net radiation.

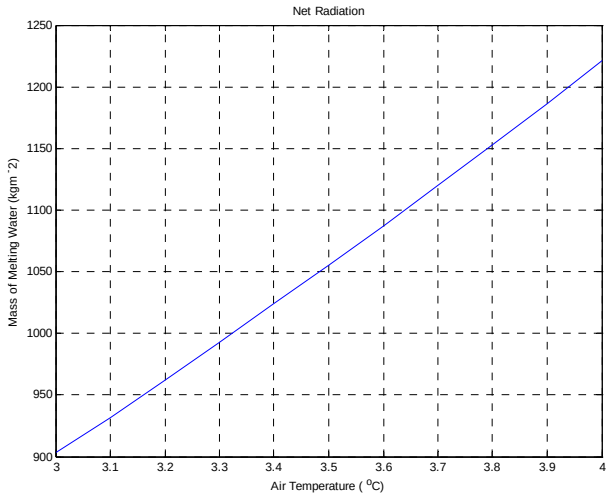

Fig 4-8: An increase in mean air temperature of 1°C during the ablation season will lead to an increase in ablation due to increase in net radiation of 318 $kg\,m^{-2}$ equivalent to 318 mm of water.

If we assume a decrease in albedo of 10% during the ablation season and hold both the Q and T constant, then Fig 4-9 shows a projection of the trend between a decrease in albedo and mass of melting water.

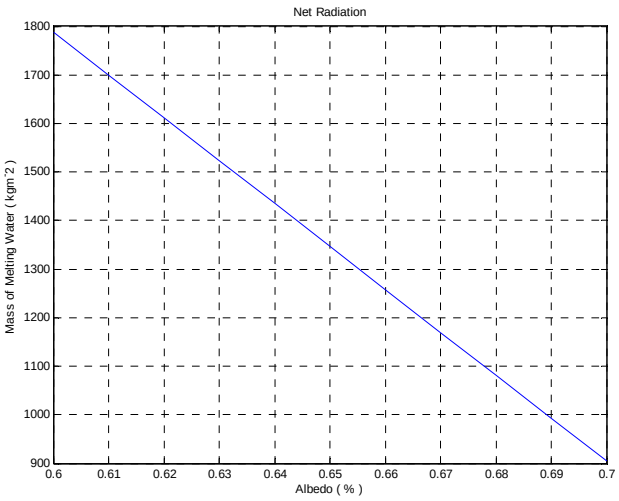

Fig 4-9: Shows that a decrease in albedo of 10% in ablation season will lead to an increase in ablation of 883 $\mathrm{kg\,m^{-2}}$ equal to 883 mm of water.

4.2.2.3 Summary of the previous section

Based on relationships between wind speed, temperature, albedo, turbulent fluxes and net radiation under standard condition the estimated total mass of melting water during the ablation season was 2272 $\mathrm{kgm^{-2}}$. The contribution from net radiation, turbulent heat fluxes of latent heat and turbulent heat fluxes of sensible heat were respectively 40%, 38% and 22% of the total mass of melting water.

A sensitivity test:

(1) An increase of the air temperature of 1°C from the mean condition in the ablation season will lead to 1161 $\mathrm{kgm^{-2}}$ higher ablation.

(2) A decrease of the albedo by 10% will lead to an increase in ablation of 883 $\mathrm{kgm^{-2}}$.

(3) An increase of the wind speed of 1 $\mathrm{ms^{-1}}$ will lead to an increase in ablation of 457 $\mathrm{kgm^{-2}}$.

4.2.3 Change in accumulation

Changes of accumulation are related to changes in annual precipitation and length of accumulation seasons which in turn, is related to air temperature. Changes in accumulation are also likely to be a result of changes in wind pattern.

Fig 1-3 showed that Lhasa experienced an annual warming in the selected period 1950-1990 of about 0.17°C/decade. In addition Fig 1-2 showed that global mean air temperature

was increasing from 1990-1999 and that the years 1990, 1991, 1995 and 1997 were particularly warm with 1999 and 2001 being two of the warmest on record. Consequently, the mean air temperature in the NyainQen TangLha during the 1990-2001 periods can be higher than that of the selected period (1950-1990).

Combining Table 4-2 and Table 4-3 a rough percentage of type of precipitation can be calculated: snow and rain are respectively 4.6%, 95.4% of the total annual precipitation.

Assume a 1°C increase in temperature; snow can be recalculated as representing just 1.1% of total annual precipitation. In addition, Fig 4-10 shows a decreasing trend of mean monthly precipitation in Lhasa between 1950 and 1990.

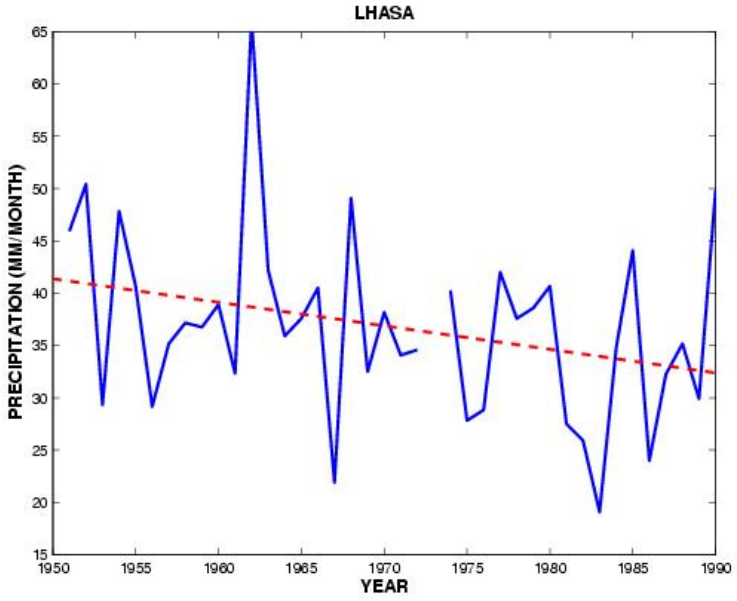

Fig 4-10: The trend of monthly mean precipitation in Lhasa during 1950-1990. (Wang La, 2003)

4.3 Change in solar elevation and the air temperature gradient

4.3.1 The effects between solar elevation, slope aspect and elevation of the fifteen glacial tongues.

In a mountainous region, slope aspect (slope angle, orientation of flow) and elevation have a great effect on the local climate, and results in different glacial changes on different slope aspects and elevations. (Changan and Jiyuan, 1992)

The range of the receding of the fifteen glacial tongues in this study was measured. The results were analysed looking for a possible relation to their different slope angle, orientation of flow and elevation. In turn, these three factors can possible be dependent on monthly short-wave radiation. The monthly short-wave irradiances are computed by the global irradiance model.

The model is run with a theoretical cloudless sky, employing standard monthly average values for precipitable water vapour, albedo and ozone. In addition an average value was selected for the latitude for the fifteen glacial tongues and also plotted into the model. Those parameters which were significant to the study were the average elevation, slope angle and orientation of each glacial tongue. The monthly irradiations are expressed as the sum of a direct beam and diffuse irradiation on the glacial tongues. Fig 4-11 shows the 12 month irradiation of the fifteen glacial tongues. The total monthly shortwave irradiance is not markedly affected by the average elevation or orientation of the fifteen glacial tongues. There are two reasons for this. Firstly, the fact that the average elevation of the fifteen glacial tongues is very high and their variation of elevation all lie within a range of just few hundred metres can be a factor.

Secondly, as the sun is higher during the ablation season in this area. This is possible also the reason for the reduced influence of orientation of flow.

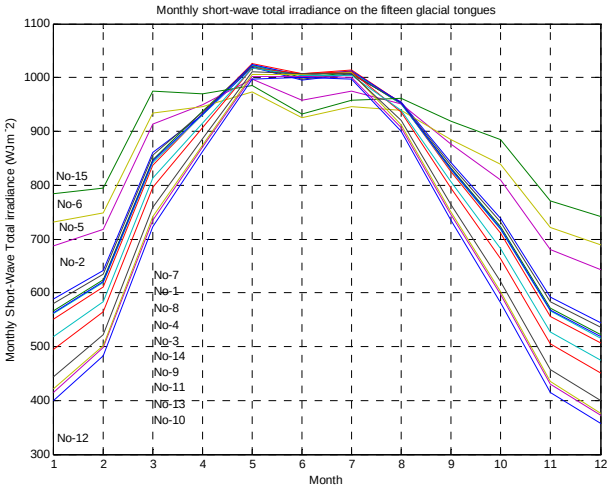

Fig 4-11: 12 month short-wave total irradiance of the fifteen glacial tongues

Fig 4-7 showed the monthly short-wave total irradiance of the fifteen glacial tongues from May to August. Fig 4-12 shows the monthly short-wave beam irradiance of the fifteen glacial tongues during the same four monthly periods. Fig 4-13 shows the monthly short-wave diffuse irradiance of the fifteen glacial tongues, again for the same four monthly periods.

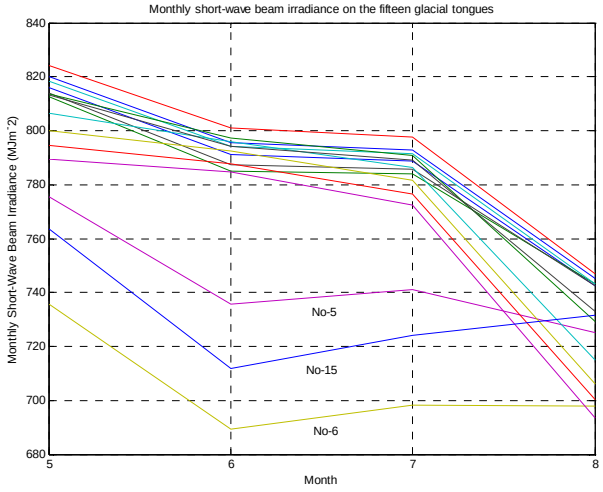

Fig 4-12: May to August monthly short-wave beam irradiance on the fifteen glacial tongues.

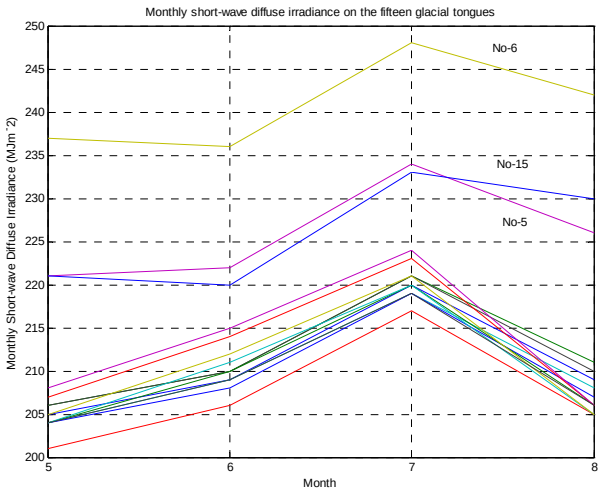

Fig 4-13: May, June, July and August monthly short-wave diffuse irradiance of the fifteen glacial tongues.

With an angle of 27.5° glacial tongue number 6 has the greatest slope angle of all fifteen. Its short-wave diffuse irradiance is also the strongest (Fig 4-13). However, this tongue's percentage of receding is the smallest, only 22%, and its monthly short-wave total irradiance (Fig 4-7) and short wave beam irradiance (Fig 4-12) is the weakest of the fifteen tongues. In addition, both the elevations of the original and present day terminus are close to the mean elevation of the fifteen glacial tongues. Its flowing orientation is from north-west to south-east.

The slope angle of glacial tongues number 5 and 15 is the second greatest of the fifteen (see Table 3-9). Their short-wave diffuse irradiance (Fig 4-13) is also the second largest. However, these tongues's monthly short-wave total irradiance (Fig 4-7), short-wave beam irradiance (Fig 4-12) and percentage of retreat (Table 3-9) are among the lowest values of all the glacial tongues with tongue number 6 being the weakest. Both the elevation of the original and present day terminus and their orientation of flow are almost the same as with tongue number 6.

The slopes of glacial tongues number 5, 6 and 15 were steep in relation to the remaining, relatively flat glacial tongues. Consequently, for these twelve flat tongues, there is no clear difference between monthly irradiance and the slope aspect. The solar elevation is high during the ablation season. Because of a more unfavourable angle of incidence for the direct beam irradiance the beam irradiation is smaller for the steep than for the flat glacier tongues (Fig 4-

12). Besides, because of an increased ground reflected irradiation, the diffuse irradiation is larger for the steep than for the flat glacier tongues (Fig 4-13). As a result the total radiation is somewhat lower for the steep than for the flat tongues (Fig 4-7) for the ablation period.

4.3.2. Relationship between the temperature gradient and the different retreat of the three parts of the glacier

The fifteen glacial tongues are separated into three parts, due to the different percentage of retreating during the 24 years. There were nine complete glacial tongues on south part of NyainQen TangLha glacier in 1977, numbers 1 to 8 and number15. The mean elevations of their original termini and present termini are 5471m and 5783m respectively. Based on table 3-9 the mean percentage of retreating is 47% during the 24 years. In addition, the topographical map clearly shows there was more snow and ice than on the other two sides compared to the south side in 1977.

Glacial tongues number 10 to 13 which were on the northern part of the mountain in 1977, no longer exist. The average elevation of these glacial tongues in 1977 and 2001 are 5654 m and 6104 m respectively. Their mean percentage of retreat is 100% since all 4 have disappeared.

In 1977, there was less snow and ice as compare to the other two parts of the glacier.

The air masses that are transported most of the humidity to this area come probably from the sector SE-SW. Where these air masses are reaching NyainQen TangLha Mountains they will be lifted. This will lead to increased precipitation on the wind side of the mountain and less precipitation on the other side. The solar height in this area (30°15`N, 90°10`E) is high. As mid summer the zenith distance of the area is 7° at midday. Differences in solar insolation of sloping North and sloping south are rather small in this area.

The remaining glacial tongues number 9 and 14 both of which were found on the southern part of the glacier in 1977 but have since experienced a retreat of 100% and no longer exist. The average elevations of their termini in 1977 and 2001 are 5706m and 6066m, respectively. This reason for these tongues disappearing may be tongues were thin.

Chapter 5

Simple model for description of the retreat of the glacier tongues of the fifteen glaciers in NyainQen TangLha

5.1 Glacier geometry

The glacial tongues of the 15 glaciers are used to test the model. Based on data from the map (Map 3-1 to 3-10) and satellite data (Fig 3-3 to 3-12). The following parameters for these 15 glaciers can be determined:

L: The total length of the glacier in 1977 (m).

α: Slope of the surface of the glacier in 1977 (degree).

ΔL: The retreat of the glacier tongue during the 24 years period 1977-2001.(m)

H_1: Elevation of glacier tongue in 1977 (m a.s.l.).

A: The total area of the glacier in 1977 (km^2).

These back ground data are given in Table 5-1:

Table 5-1: Back ground data for the 15 glacier tongues.

Glacial tongue	L (m)	Δ L (m)	α (degree)	H_1 (m.a.s.l)
No-1	6180	2930	8.5	5250
No-2	6390	4780	5.7	5250
No-3	11310	7830	3.5	6090
No-4	3370	1670	3.4	5440
No-5	2040	520	21.2	5440
No-6	2800	620	27.5	5400
No-7	3880	2140	7.5	5200
No-8	2870	1850	7.4	5480
No-9	4470	4410	5.7	5520
No-10	3140	3140	11.5	5400
No-11	860	790	8.6	5680
No-12	2710	2710	13.3	5640
No-13	2050	2050	11.1	5890
No-14	1990	1990	8.4	5890
No-15	1650	380	17.4	5860

Due to the general lack of back ground data we have to make some assumption had to be made for the simplification of the model.

5.1.1 Ice thickness

A. There exist a relationship between the mean ice thickness h of the glacier and the area A. This relationship is given by Mool (2000).

$$h = -11.32+53.21\ A^{0.3} \quad (m) \qquad (5.1)$$

Here A is the total area of the glacier (km^2). This formula has been used to estimate the mean ice thickness in the glacier inventory of the Bhutan Himalayas. The same method is also used here to find the ice thickness. An empirical relation like Eq (5.1) will probably be dependant of the slope of the bedrock.

B. Muller (1977) described a relationship between mean ice thickness for various glaciers types, forms, and areas (see Fig 5-1). This method was also used in our study to determine the mean values of the ice thickness of the 15 glacial tongues. The results are given in Table 5-2. It is clear from Table 5-2 that method **A** results in estimations of ice thickness greater than that of method **B.**

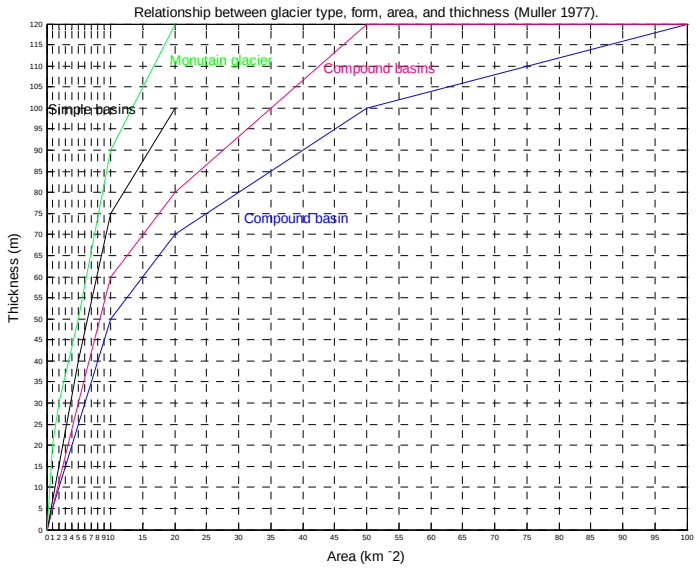

Fig 5-1: The relationship between area and ice thickness. Ice thickness depended also on glacier type and form (Muller, 1977).

Table 5-2. The thickness of the fifteen glacial tongues, using the aforementioned methods.

Glacial number	1	2	3	4	5	6	7	8	9	10	11	12	13	14	15
The total area of the glacier A (km^{-2})	3.4	2.2	14.4	2.4	3.1	2.2	1.3	2	3.4	2.5	1.4	1.8	2.3	2.3	0.8
A. The mean ice thickness H (m)	66	56	107	58	63	56	46	54	66	59	48	52	57	57	38
B. The mean ice thickness H (m)	25	17	77	19	22	17	12	16	25	20	13	15	18	18	9

5.1.2 Deformation velocity / no sliding

We assume that the sliding velocity can be ignored because of the low shear stress in the layer between ice and rock (see Table 5-3). That means that the deformation velocity u can be expressed:

$$u = \frac{2\overset{o}{A}}{n+2}\tau_b^n h \qquad \text{(m)} \qquad (5.2)$$

Where

$$\tau_b = \rho g h \sin(\gamma) \quad \text{(kPa)} \qquad (5.3)$$

Here

$\overset{o}{A}$ is a flow parameter which here is taken as equal to $6.8 \cdot 10^{-15}$ $(kPa)^{-3} \cdot s^{-1}$ for temperate ice and n is assumed to be equal to 3 (Duval, 1977).

h is the mean thickness of the glacier based on Eq (5.1) and Fig 5-1.

τ_b is the bottom shear stress (kPa). g is the acceleration of gravity and γ is the slope of the bedrock. Fig 5-2 shows a simple cross section of a length profile of the glacier.

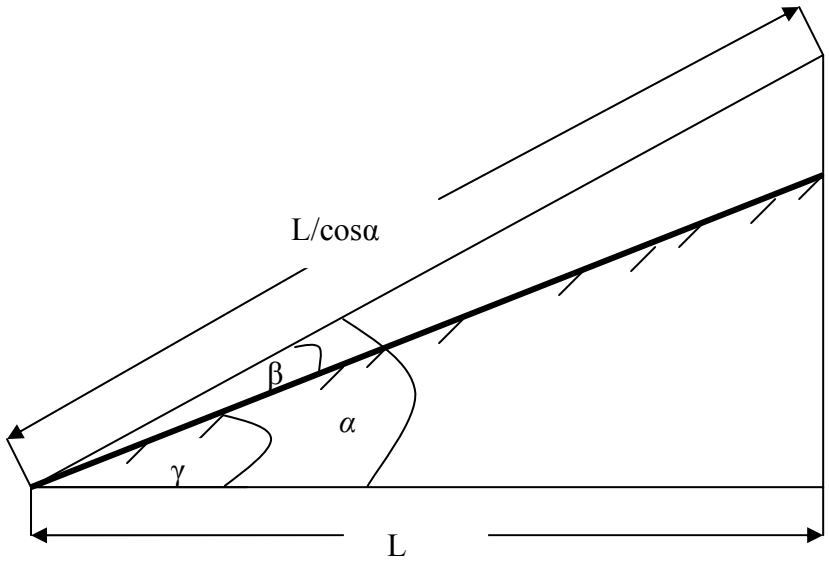

Fig 5-2: A simple cross section of a length profile of the glacier. Here γ is the slope of the bedrock and α is the slope of the surface of the glacier which is taken from Map 3-1 to 3-10.

5.1.3 Slope angle of bedrock

The angle β which is equal to the angle between the ice surface and the bedrock can be calculated in the following way (Fig 5-3):

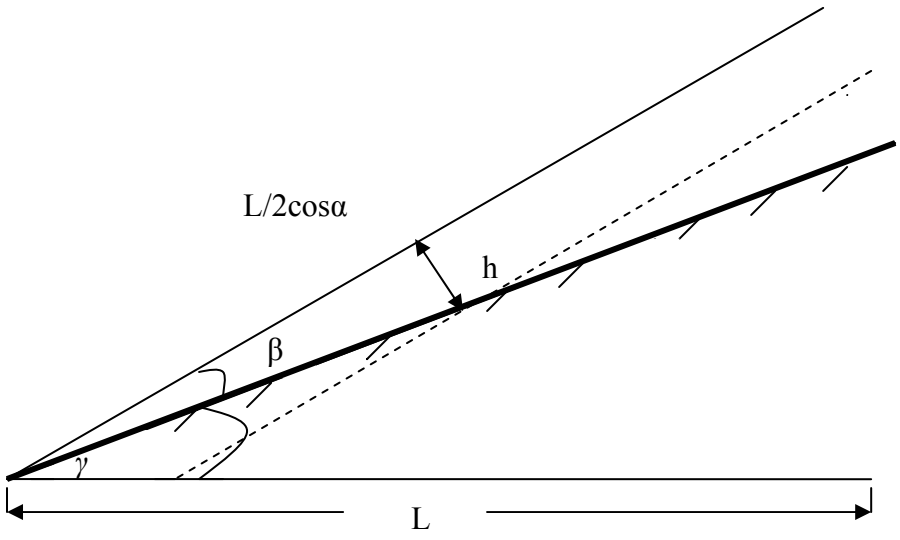

Fig 5-3. A way of calculation of the angle β.

If we assume that the surfaces of the glaciers are rectangular the mean thickness of the glacier will correspond to $\frac{L}{2\cos\alpha}$ (Fig 5-3). We then get:

$$\tan\beta \approx \sin\beta = \frac{h}{\frac{L}{2\cos\alpha}} \qquad (5.4)$$

The slope of the bedrock γ can then be determined:

$$\gamma = \alpha - \beta \qquad (5.5)$$

The calculated data so far for the 15 glaciers are given in Table 5-3.

Table 5-3: The data of the 15 glacial tongues are calculated so far. The annual rate of melting S is equal to 2272 $kg \cdot m^{-2} \cdot yr^{-1}$ and are the same for all the glacial tongues. The different values are calculated using **A.** ice thickness based on Eq 5.1 and **B.** ice thickness based on Fig 5-1.

Number of glacier	1	2	3	4	5	6	7	8	9	10	11	12	13	14	15
A. The angle between surface and bedrock β	1.2	1	1	2	3	2	1.3	2	1.7	2	6.3	2	3	3.4	2.5
B. The angle between surface and bedrock β	0.5	0.3	0.8	0.6	1.2	0.8	0.4	0.6	0.5	0.6	1.7	0.6	0.8	1	0.7
A The slope of the bedrock γ	7.3	4.7	2.5	1.4	18	26	6.2	5.4	4	9.5	2.3	11	8.1	5.3	15
B. The slope of the bedrock γ	8	5.4	2.7	2.8	20	27	7.2	6.8	5.2	11	6.9	13	10	7.4	17
A. Bottom shear stress τ_b (kPa)	77	42	43	13	179	225	46	47	42	89	18	91	74	47	90
B. Bottom shear stress τ_b (kPa)	32	15	33	9	69	71	14	17	20	35	14	31	29	21	24
A. Deformation velocity u $(m \cdot yr^{-1})$	2.6	0.4	0.7	0.01	31	54	0.4	0.5	0.4	3.6	0.02	3.4	2	0.5	2.4
B. Deformation velocity u $(m \cdot yr^{-1})$	0.7	0.005	0.2	0.001	0.6	0.5	0.003	0.007	0.02	0.07	0.003	0.04	0.04	0.01	0.01

We consider the lower part of the ablation area and we assume that the annual rate of melting S ($kg \cdot m^{-2} \cdot yr^{-1}$) (calculated in **Chapter 4)** and the mean rate of accumulation D ($kg \cdot m^{-2} \cdot yr^{-1}$) are the same for the lowest part of the glaciers.

The net lose of ice during 24 years is expressed as mass of ice W ($kg \cdot m^{-2}$).

$$W = (S - D) \cdot 24 \quad (kg \cdot m^{-2}) \qquad (5.6)$$

5.2 Retreats from 1977 to 2001.

In Fig 3-3 to 3-12 a model was developed to calculate the annual melting (S) during the 24 year. A simple model will now be used to calculate the thickness of the glacier tongue (Fig 5-4).

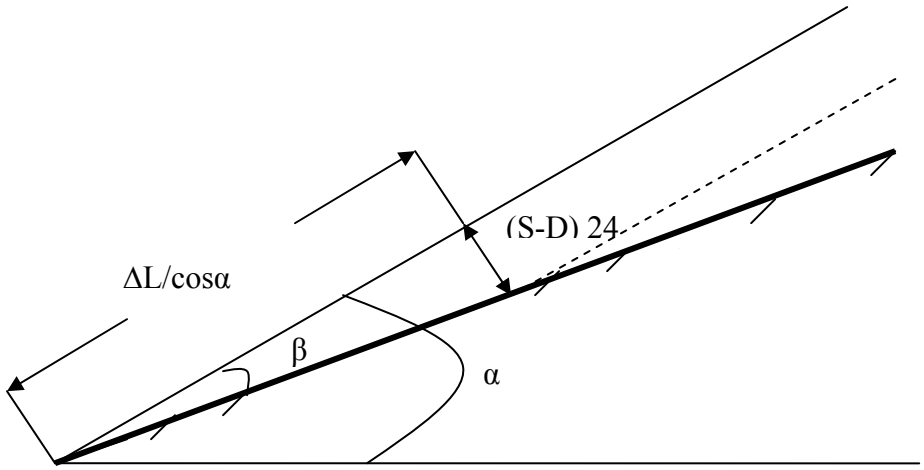

Fig 5-4: A simple model of a glacial tongue.

Based on Fig 5-4 and take into consideration the flow of the glacier we get the following equation.

$$(\frac{\Delta L}{\cos\alpha} - u \cdot 24) \sin\beta = (S-D) \cdot 24 \qquad (5.7)$$

This can be written

$$\Delta L = 24 \cdot (\frac{S - D}{\sin\beta} + u) \cos\alpha \qquad (m) \qquad (5.8)$$

Here the rate of accumulation is not measured and can be calculated based on (Eq (5.8)).

$$S\text{-}D = \frac{\Delta L \sin\beta}{24 \cos\alpha} + u \sin\beta \qquad (5.9)$$

$$D = S- \left(\frac{\Delta L}{24\cos\alpha}+u\right)\sin\beta \qquad (5.10)$$

Table 5-4 shows the rate of the accumulation of the glacial tongues as is calculated using Eq (5.10).

Table 5-4: The rate of the accumulation of the glacial tongues. The different values are calculated using A. ice thickness based on Eq (5.1) and B. ice thickness based on Fig 5-1.

Number of glacier	**A.** The rate of accumulation D ($kg \cdot m^{-2} \cdot yr^{-1}$)	**B.** The rate of accumulation D ($kg \cdot m^{-2} \cdot yr^{-1}$)
1	-387	1279
2	-1216	1211
3	-3922	-2178
4	-125	1485
5	-842	1797
6	-664	1872
7	-152	1724
8	-654	1415
9	-3172	794
10	-2779	805
11	-1427	1271
12	-2191	1020
13	-2584	1054
14	-2511	770
15	1436	2069

The rate of accumulation is calculated using Eq (5.10). Where L and ΔL are determined by use of topographic maps and satellite images. u is deformation velocity ($m \cdot yr^{-1}$) of the glacier $24 \cdot u$ is therefore the total displacement over the 24 year period which is smaller than ΔL. h is taken from Eq (5.1) and Fig 5-1.

Table 5-4 shows that the rate of the accumulation of the glacial tongue No-3 is negative under both the method **A** and method **B**. Values may depend on the rate of the ablation and the ice thickness. There are maybe a couple of reasons for this. (1) The rate of the ablation was calculated using the mean conditions during the ablation season (ie. Temperature, $3\,^{0}\mathrm{C}$, wind speed, $3\ \mathrm{m\,s^{-1}}$, relative humidity, 100% and albedo, 70%). There is a possibility that this value was too small for tongue No-3. (2) h was calculated using Eq (5.1) and Fig 5-1. This value could have been too large.

According to the results given in Table 5-4 we conclude that only method **B** for determination of accumulation D is realistic. Except for glacier 3 the calculated rate of accumulation varies from 794-2068 ($\mathrm{kgm^{-2}\ yr^{-1}}$). Fig 5-5 shows the very weak relationship between the rate of accumulation and height of glacier tongues.

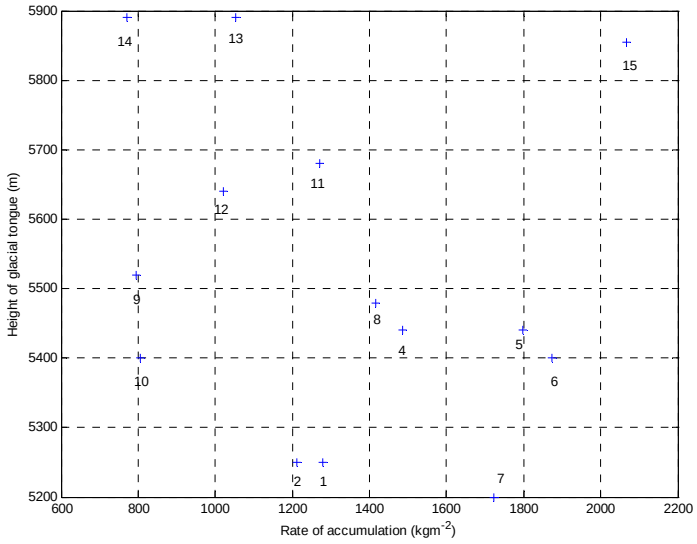

Fig 5-5: A relationship between height of glaciers and the rate of the accumulations. (calculated based on Eq (5.10)).

Chapter 6

Estimating the mass balance in the future based on different climatic scenarios.

6.1 Back ground data

Glaciers No-1, 6, 11 and 15 have been chosen to calculate glacial retreat under different climatic scenarios. The mean climatic conditions in the ablation season were estimated to be a temperature of $3\,^{0}\mathrm{C}$, a wind speed of $3\ \mathrm{m\,s^{-1}}$, a relative humidity of 100% and an albedo of 70%.

The following parameters from earlier in this study have been used in this section to calculate the effect of different climatic scenarios:

ΔL: retreat of glacier tongue during the 24 year period 1977-2001 (see Table 6-1).

β: angle between the ice surface and bedrock (Table 5-3).

α: Slope of the surface of the glacier (Table 5-1)

S: rate of the ablation under mean climatic conditions. S is taken as the same value for all the glacial tongues in this calculation.

u: deformation velocity (Table 5-3).

D: rate of the accumulation (Table 5-4).

L: total length of glacier in 1977 (see Table 6-1).

Table 6-1: Total length for the four glacial tongues.

Glacial tongue	No-1	No-6	No-11	No-15
L (m)	6180	2800	860	1650
ΔL (m)	2930	620	790	380

6.2 Climatic scenarios

6.2.1 No change

Here the mean climatic conditions were used to calculate the time taken (t) for the entire glacial tongues to retreat and disappear t is derived used Eq (5.8).

$$L=t\cdot\left(\frac{S-D}{\sin\beta}+u\right)\cdot\cos\alpha \quad \text{(m)} \tag{6.1}$$

This can be written

$$t=L/\left[\left(\frac{S-D}{\sin\beta}+u\right)\cdot\cos\alpha\right] \quad \text{(years)} \tag{6.2}$$

Inserting numbers from Table 5-1, 5-3, 5-4 and Eq (5.2) we find:

Glacier No-1: t = 50 years

Glacier No-6: t = 108 years

Glacier No-11: t = 26 years

Glacier No-15: t =104 years

6.2.2 Change air temperature

Here air temperature is increased by 1°C whilst other climatic variables, D and u are held constant in order to estimate the extent to which the glacial tongue could have retreated (ΔL_1) in the period 1977-2001. Earlier, it was found (4.2.2.3) that a 1°C increase in temperature would lead to an increase in ablation from 2272 $kgm^{-2}\ yr^{-1}$ to 3434 $kgm^{-2}\ yr^{-1}$ (S_1). Using this new rate of ablation ΔL_1 can be calculated using Eq (6.1).

$$\Delta L_1=24\cdot\left(\frac{S_1-D}{\sin\beta}+u\right)\cdot\cos\alpha \ \text{(m)} \tag{6.3}$$

Inserting numbers from Table 5-1, 5-3, 5-4 and Eq (5.2) we find:

Glacier No-1: ΔL_1 = 6408 (m)

Glacier No-6: ΔL_1 = 2391 (m)

Glacier No-11: ΔL_1 = 1716 (m)

Glacier No-15: ΔL_1 = 2557 (m)

By comparing the values of ΔL_1 with the corresponding lengths in 1977 (L), we see that all but one of the glacial tongues could have disappeared completely with a 1°C increase in air

temperature. Glacial tongue No-6 remains since $\Delta L_1 < L$ (see Table 6-1). Fig 6-1 shows the length of glacial tongue No-6 with and without the temperature increase.

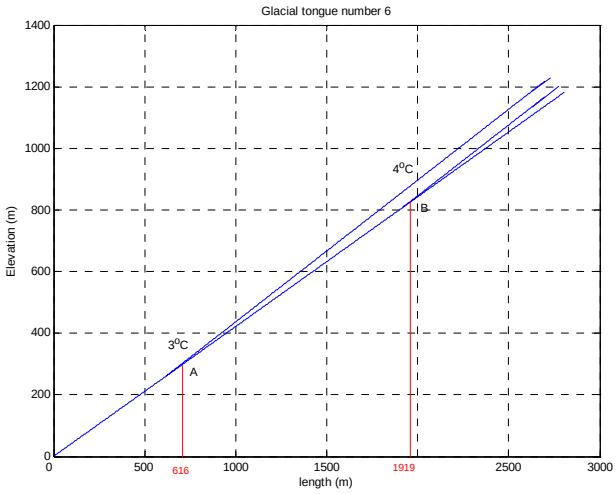

Fig 6-1: Length of glacial tongue No-6 with mean air temperature of A, 3°C and B, 4°C other climatic conditions are held constant.

6.2.3 Change Albedo

Here albedo is decreased by 10% while other climatic variables, D and u are held constant in order to estimate the extent to which the glcial tongue could have retreated ΔL_2 in the period 1977-2001. Earlier, it was found (4.2.2.3) that a 1°C increase in temperature would lead to an increase in ablation from 2272 kgm^{-2} yr^{-1} to 3155 kgm^{-2} yr^{-1} (S_2). Using this new rate of ablation ΔL_2 can be calculated using Eq (6.1).

$$\Delta L_2 = 24 \cdot \left(\frac{S_2 - D}{\sin \beta} + u \right) \cdot \cos\alpha \ (m) \qquad (6.4)$$

Inserting numbers from Table 5-1, 5-3, 5-4 and Eq (5.2) we find:

Glacier No-1: $\Delta L_2 = 5583m$

Glacier No-6: $\Delta L_2 = 1967m$

Glacier No-11: $\Delta L_2 = 1496m$

Glacier No-15: $\Delta L_2 = 2036$ m

By comparing the values of ΔL_2 with values of L, we see that glacial tongues No-11 and No-15 could have disappeared as a result of a decrease in albedo (Fig 6-2) shows the length of the glacial tongue which would have remained.

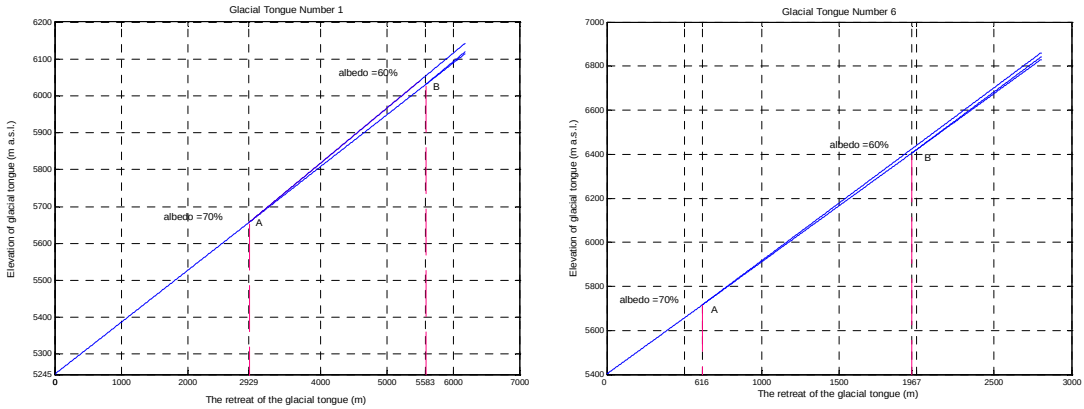

Fig 6-2 Length of glacial tongues No-1 and No-6 with an albedo of A, 70% and B, 60% other climatic conditions are held constant.

6.2.4 Change wind speed

Here wind speed is increased by 1 ms^{-1} whilst other climatic variables, D and u are held constant in order to estimate the extent to which the glacial tongue could have retreated (ΔL_3) in the period 1977-2001. Earlier, it was found (4.2.2.3) that a 1 ms^{-1} increase in wind speed would lead to an increase in ablation from 2272 kgm^{-2} yr^{-1} to 2729 kgm^{-2} yr^{-1} (S_3). Using this new rate of ablation ΔL_3 can be calculated using Eq (6.1).

$$\Delta L_3 = 24 \cdot \left(\frac{S_3 - D}{\sin \beta} + u \right) \cdot \cos\alpha \quad (m) \qquad (6.5)$$

Inserting numbers from Table 5-1, 5-3, 5-4 and Eq (5.2) we find:

Glacier No-1: $\Delta L_3 = 4319$ m

Glacier No-6: $\Delta L_3 = 1318$ m

Glacier No-11: $\Delta L_3 = 1158$ m

Glacier No-15: $\Delta L_3 = 1260$m

By comparing values of ΔL_3 with values of L it becomes apparent that just one of the four glacial tongues, No-11 would have disappeared ($\Delta L_3 > L$) as a result of this increase in wind speed, Fig 6-3 shows the lengths of the glacial tongues that have remained.

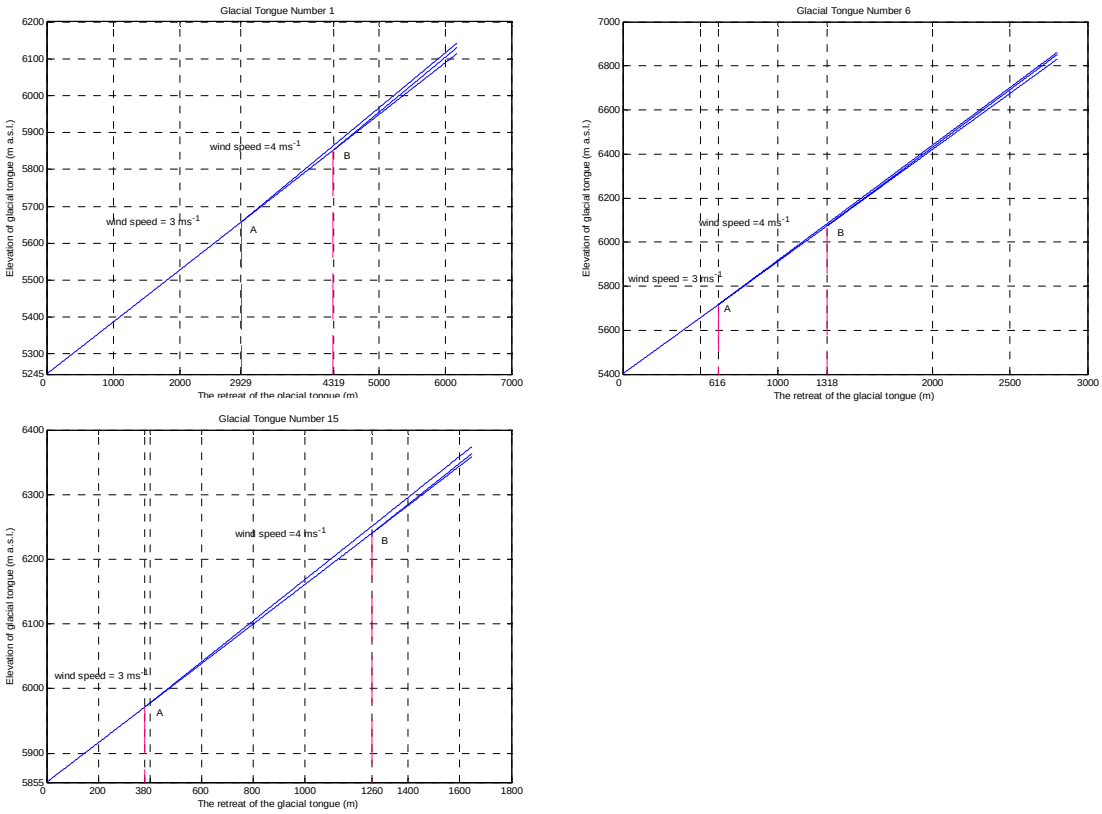

Fig 6-3: Length of glacial tongues No-1, No-6 and No-15 where wind speed is taken as A, 3 ms^{-1} and B, 4 ms^{-1}, other climatic conditions are held constant.

Chapter 7

Summary and conclusions

The extent of the 15 glacial tongues in the Mount NyainQen TangLha area in Tibet, were determined from original topographic maps from 1977, and from satellite data (ASTER SWIR) 24 years later.

The data from the original topographical map employing both the geographical coordinate system and the map coordinate system were transformed by a matlab program (Asterpoint) to the satellite image coordinate system, corresponding to the ASTER satellite data.

The Aster-data was used to plot the extent of the fifteen glacial tongues by employing the matlab program (Swirsubreg). In the processing, DN limiting value was chosen to be 60.

Retreats were observed for all the glacial tongues. The mean retreat of the glacial tongues that are facing to SE-S is 105 my^{-1}. It is not possible to know when the glaciers facing to the sector E-NW-N disappeared. The total areas of the glacial tongues were 45.5 km^{-2} in 1977 being reduced to 20.1 km^{-2} in 2001.

Based on the data from meteorological stations in the district with positions 3000-4000m above sea-level, the temperature in the area of the glacier was calculated using mean temperature lapse rate of $0.65\,^{0}C/100m$. The mean relative humidity in Lhasa (3760 m.a.s.l.) during ablation season is about 80%. It was therefore estimated to be 100% in the study area. A mean wind speed was estimated to be 3 ms^{-1}. The albedo for the surface of the glacier was taken to be 70%.

Based on the relationships between wind speeds, temperature, albedo, turbulent fluxes and net radiation under standard condition the estimated total mass of melting water during the ablation season was 2300 $kg\,m^{-2}\,yr^{-1}$. The turbulent fluxes of sensible heat and latent heat contributed to 22% and 38% of the total ablation, respectively. The remaining 40% of ablation was a result of radiation.

Sensitivity tests were carried out in order to approximate the effect that different climatic and environmental factors could have on the rate of ablation. An increase of the air temperature of $1\,^{0}\mathrm{C}$ from the mean conditions in the ablation season would lead to an increase of 1200 $\mathrm{kg\,m^{-2}}$ higher ablation. An increase of wind speed of $1\mathrm{m\,s^{-1}}$ would lead to 500 $\mathrm{kg\,m^{-2}}$. A decrease in albedo of 10% would lead to an increase in ablation of 900 $\mathrm{kg\,m^{-2}}$.

By application of a simple model the mean thickness of the glacial tongues was found to be 15 m. Except for glacier 3 the calculated rate of accumulation varies from 800-2100 ($\mathrm{kgm^{-2}\,y^{-1}}$) and the mean rate of accumulation was calculated to be 1100 $\mathrm{kg\,m^{-2}}$

The different climatic scenarios and the aforementioned sensitivity tests illustrate the most important climatic and environmental factors which have resulted in the retreat of the NyainQen TangLha glacier.

Appendix A

A.1 Geolaloswir

```
function [lati,long] = geolaloswir(I,J);
%gives latitude and longitude for line number I and pixel number J
%number of lines is 2100 (I=0-2099), number of pixels is 2490 (J=0-2489)
%NOTE THAT LINES ARE COUNTED FROM NORTH TO SOUTH (pixels from west to
east)
%first step: grid cell location (indices given by iloc+1 and jloc+1)
%and local indices (ip,jp)
%second step: find lati and long by interpolation
format long
incpix=249;
inclin=210;
jloc=floor(J/incpix);
jp=J-jloc*incpix+1;   %to avoid index=0
iloc=floor(I/inclin);
ip=I-iloc*inclin+1;   %to avoid index=0
%
% Read geolocation fields
%
cd /Data/data8/dongc
file_id=hdfsw('open','AST_06S_00311202001045037000000.hdf','read');
swath_id=hdfsw('attach',file_id,'DecorrelationStretchSWIR');
[data2,status2]=hdfsw('readfield',swath_id,'GeodeticLatitude',[],[],[]);
LAT=data2';
[data3,status3]=hdfsw('readfield',swath_id,'Longitude',[],[],[]);
LONG=data3';
status=hdfsw('detach',swath_id);
status=hdfsw('close',file_id);
cd /home5/dongc/GLACIER
%coordinates of corner points:
```

```
%matlab does not like index=0, therefore iloc and jloc must be adjusted by 1
%nw is northwest, ne is northeast, sw is southwest, and se is southeast
nwlat=LAT(iloc+1,jloc+1);nwlon=LONG(iloc+1,jloc+1);
nelat=LAT(iloc+1,jloc+2);nelon=LONG(iloc+1,jloc+2);
swlat=LAT(iloc+2,jloc+1);swlon=LONG(iloc+2,jloc+1);
selat=LAT(iloc+2,jloc+2);selon=LONG(iloc+2,jloc+2);
%
%the north and south edge
for j=1:incpix;
noedlat(j)=(nwlat*(incpix-j)+nelat*(j-1))/(incpix-1);
noedlon(j)=(nwlon*(incpix-j)+nelon*(j-1))/(incpix-1);
soedlat(j)=(swlat*(incpix-j)+selat*(j-1))/(incpix-1);
soedlon(j)=(swlon*(incpix-j)+selon*(j-1))/(incpix-1);
end
%the west and east edge
for i=1:inclin;
weedlat(i)=(nwlat*(inclin-i)+swlat*(i-1))/(inclin-1);
weedlon(i)=(nwlon*(inclin-i)+swlon*(i-1))/(inclin-1);
eaedlat(i)=(nelat*(inclin-i)+selat*(i-1))/(inclin-1);
eaedlon(i)=(nelon*(inclin-i)+selon*(i-1))/(inclin-1);
end
%latitude and longitude for line number I and pixel number J
%(line number ip and pixel number jp in the local grid cell)
%first an interpolation in the eastern direction
lati1=(weedlat(ip)*(incpix-jp)+eaedlat(ip)*(jp-1))/(incpix-1);
long1=(weedlon(ip)*(incpix-jp)+eaedlon(ip)*(jp-1))/(incpix-1);
%
%then in the southern direction
lati2=(noedlat(jp)*(inclin-ip)+soedlat(jp)*(ip-1))/(inclin-1);
long2=(noedlon(jp)*(inclin-ip)+soedlon(jp)*(ip-1))/(inclin-1);
%
% take their mean to output
%
lati=0.5*(lati1+lati2);
```

```
long=0.5*(long1+long2);
```

A.2 Geogrid

```
function [gnorth,geast]=geogrid(lati,long);
% gives grid position (gnorth,geast) on map for a given pair of latitude
% and longitude (lati,long).
% 30.00<lati<30.67 and 90.00<long<91.00
%
% Corner points coordinates:
% Southwest:
swlat=30.00; swlon=90.00;
swgnorth=23.85; swgeast=10.50;
% Southeast:
selat=30.00; selon=91.00;
segnorth=21.88; segeast=106.99;
% Northwest:
nwlat=30.66667; nwlon=90.00;
nwgnorth=97.78; nwgeast=12.52;
%Northeast:
nelat=30.66667; nelon=91.00;
negnorth=95.78; negeast=108.31;
%
% first step: determine the coordinates of the edge points belonging
% to the input point:
%
% Edge point to the north:
weight1=(nelon-long)/(nelon-nwlon);
weight2=(long-nwlon)/(nelon-nwlon);
edgeno_gnorth=nwgnorth*weight1+negnorth*weight2;
edgeno_geast=nwgeast*weight1+negeast*weight2;
%
% Edge point to the south:
edgeso_gnorth=swgnorth*weight1+segnorth*weight2;
```

```
edgeso_geast=swgeast*weight1+segeast*weight2;
%
% Edge point to the west:
weight1=(nwlat-lati)/(nwlat-swlat);
weight2=(lati-swlat)/(nwlat-swlat);
edgewe_gnorth=swgnorth*weight1+nwgnorth*weight2;
edgewe_geast=swgeast*weight1+nwgeast*weight2;
%
% Edge point to the east:
edgeea_gnorth=segnorth*weight1+negnorth*weight2;
edgeea_geast=segeast*weight1+negeast*weight2;
%
% Second step determine the coordinates of the input point
%
% North-south:
weight1=(nwlat-lati)/(nwlat-swlat);
weight2=(lati-swlat)/(nwlat-swlat);
gnorth1=edgeso_gnorth*weight1+edgeno_gnorth*weight2;
geast1=edgeso_geast*weight1+edgeno_geast*weight2;
%
% East-west:
weight1=(nelon-long)/(nelon-nwlon);
weight2=(long-nwlon)/(nelon-nwlon);
gnorth2=edgewe_gnorth*weight1+edgeea_gnorth*weight2;
geast2=edgewe_geast*weight1+edgeea_geast*weight2;
%
% Take the mean of the two estimates
%
gnorth=0.5*(gnorth1+gnorth2)
geast=0.5*(geast1+geast2)
```

A.3 Asterpoint

```
function [err_vici,line,pixel,lat,lon]=asterpoint(gno,gea);
%
% gives line and pixel of ASTER SWIR data, and also it
% gives geographic position (lat,lon) on map for a given grid position
% (gno,gea)
%
% 21.88<gno<97.78 and 10.50<gea<108.31
%
%
% Read geolocation fields
%
cd /data1/barthel/caidong
file_id=hdfsw('open','AST_06S_00311202001045037000000.hdf','read');
swath_id=hdfsw('attach',file_id,'DecorrelationStretchSWIR');
[data2,status2]=hdfsw('readfield',swath_id,'GeodeticLatitude',[],[],[]);
LAT=data2';
[data3,status3]=hdfsw('readfield',swath_id,'Longitude',[],[],[]);
LONG=data3';
status=hdfsw('detach',swath_id);
status=hdfsw('close',file_id);
cd /home5/barthel/caidong
%
% Corner points coordinates:
% Southwest:
swlat=30.00; swlon=90.00;
swgnorth=23.85; swgeast=10.50;
% Southeast:
selat=30.00; selon=91.00;
segnorth=21.88; segeast=106.99;
```

```
% Northwest:
nwlat=30.66667; nwlon=90.00;
nwgnorth=97.78; nwgeast=12.52;
%Northeast:
nelat=30.66667; nelon=91.00;
negnorth=95.78; negeast=108.31;
%
% first step: determine the coordinates of the edge points belonging
% to the input point:
%
% Edge point to the north:
weight1=(negeast-gea)/(negeast-nwgeast);
weight2=(gea-nwgeast)/(negeast-nwgeast);
edgeno_lat=nwlat*weight1+nelat*weight2;
edgeno_lon=nwlon*weight1+nelon*weight2;
edgeno_gno=nwgnorth*weight1+negnorth*weight2;
%
% Edge point to the south:
weight1=(segeast-gea)/(segeast-swgeast);
weight2=(gea-swgeast)/(segeast-swgeast);
edgeso_lat=swlat*weight1+selat*weight2;
edgeso_lon=swlon*weight1+selon*weight2;
edgeso_gno=swgnorth*weight1+segnorth*weight2;
%
% Edge point to the west:
weight1=(nwgnorth-gno)/(nwgnorth-swgnorth);
weight2=(gno-swgnorth)/(nwgnorth-swgnorth);
edgewe_lat=swlat*weight1+nwlat*weight2;
edgewe_lon=swlon*weight1+nwlon*weight2;
edgewe_gea=swgeast*weight1+nwgeast*weight2;
%
% Edge point to the east:
weight1=(negnorth-gno)/(negnorth-segnorth);
weight2=(gno-segnorth)/(negnorth-segnorth);
```

```
edgeea_lat=selat*weight1+nelat*weight2;
edgeea_lon=selon*weight1+nelon*weight2;
edgeea_gea=segeast*weight1+negeast*weight2;
%
% Second step determine the coordinates of the input point
%
% North-south:
weight1= (edgeno_gno-gno)/ (edgeno_gno-edgeso_gno);
weight2= (gno-edgeso_gno)/ (edgeno_gno-edgeso_gno);
lat1=edgeso_lat*weight1+edgeno_lat*weight2;
lon1=edgeso_lon*weight1+edgeno_lon*weight2;
%
% East-west:
weight1= (edgeea_gea-gea)/ (edgeea_gea-edgewe_gea);
weight2= (gea-edgewe_gea)/ (edgeea_gea-edgewe_gea);
lat2=edgewe_lat*weight1+edgeea_lat*weight2;
lon2=edgewe_lon*weight1+edgeea_lon*weight2;
%
% Take the mean of the two estimates
%
lat=0.5*(lat1+lat2)
lon=0.5*(lon1+lon2)
%
% iteration procedure to find line and pixel
%
epsil=1e-3;
I=1800;J=500; % first guess
[lati,long]=laloswir(I,J,LAT,LONG);
error=sqrt((lati-lat)^2+(long-lon)^2);
err_line=lati-lat;
err_pix=long-lon;
while error > epsil
%
if err_line < 0
```

```
I=I-1;
[lati,long]=laloswir(I,J,LAT,LONG);
err_line=lati-lat;
end
if err_line > 0
I=I+1;
[lati,long]=laloswir(I,J,LAT,LONG);
err_line=lati-lat;
end
if err_pix < 0
J=J+1;
[lati,long]=laloswir(I,J,LAT,LONG);
err_pix=long-lon;
end
if err_pix > 0
J=J-1;
[lati,long]=laloswir(I,J,LAT,LONG);
err_pix=long-lon;
end
%
error=sqrt((lati-lat)^2+(long-lon)^2);
end
% we are now in the vicinity of the solution
% next we find the minimum which gives the best fit
%
radius=10;
min_err=error;
for n=-radius:radius;
   II=I+n;
   for m=-radius:radius;
      JJ=J+m;
      [lati,long]=laloswir(II,JJ,LAT,LONG);
      error=sqrt((lati-lat)^2+(long-lon)^2);
      err_vici(n+radius+1,m+radius+1)=error;
```

```
        if error < min_err
            line=II;
            pixel=JJ;
        end
    end
end
min(min(err_vici))
line
pixel
```

A.4 Swirsubreg

```
function [cswir,S]=swirsubreg(IX,IY)
% subregion defined by pixel, IX(=0-2489), and line IY(=0-2099)
% returns contour plot cswir, and the data subset S.
%
% open and read the data, then close the data file, and return to home directory
%

cd /Data/data8/dongc

file_id=hdfsw('open','AST_06S_00311202001045037000000.hdf','read');
swath_id=hdfsw('attach',file_id,'DecorrelationStretchSWIR');
[DT,status]=hdfsw('readfield',swath_id,'Band9',[],[],[]);
D=DT';%matlab convention makes it necessary to take the transpose
status=hdfsw('detach',swath_id);
status=hdfsw('close',file_id);
cd /home5/dongc/GLACIER
% dissmiss the abundant data
clear DT
Y=-IY;%because lines are counted from north to south, and
%matlab axes values must increase upward
X=IX;
```

```
%indices must be increased by one because matlab does not like zero
%as index value
S=double(D(IY(1)+1:IY(end)+1,IX(1)+1:IX(end)+1));
[i,j]=meshgrid(X,Y);
figure
[cswir, h] =contourf(i,j,S);
%set(h, 'linewidth', 1);
```

Bibliography

Abrams, M., 2000, The Advanced Spaceborne Thermal Emission and Reflection Radiometer (ASTER): Data products for the high spatial resolution imager on NASA's Terra platform. International Journal of Remote Sensing, 21(5): 847-859.

Ahrens, C. D., 1999, METEOROLOGY TODAY, v. 5 p. 116-119.

Ahrens, C. D., 1999, METEOROLOGY TODAY, v. 9 p. 221-223.

Ahlman, H. W., 1935a, Contribution to the physics of glaciers. *Geogr. J.*, 86, 97-113. [9]

Alt, B. T., 1975, The energy Balance of Meighen Ice Cap, N. W. T., Vols. 1 and 2. Polar Continental Shelf project, Department of Energy, Mines and resources, Ottawa, Canada. [63]

Arai, K., 2001, Early results from the vicarious calibration of Terra/ASTER/SWIR, Claibretion and Characterization of Satellite Sensors and Accuracy of Derived Physical Parameters. 28: 77-82.

Changan, S and Jiyuan, L., 1992, Studies of Glacier Change during Quaternary Period in Tibet by using Ramote Sensing and GIS Techniques, Gisdevelopment.net p.1-3.

Czeplak, G. and Kasten. F., 1987, Parametrsierung der atmosphärischen Wärmestrahlung bei bewölktem Himmel. *Met. Rundschau* 6, 184-187.

Duval, P., 1977, The role of water content on the creep rate of polycrystalline ice. *IAHS*, 27, 129-40

Dyurgerov, M. B. and M. Meier. 1997. Mass balance of mountain and sub-polar glaciers: A new global assessment for 1961-1990, Arctic and Alpine Research, 29 (4), 379-391.

Easterbrook, D.J., 1999, Surface processes and landforms, v. 12 p. 303-310.

Haeberli, W., 1995.Glacier fluctuations and climate change detection - operational elements of worldwide monitoring strategy. WMO Bulletin Vol. 44, No. 1, S. 23-31.

Haeberli, W. and Hoelzle, M., 1995, Application of inventory data for estimating characteristics of and regional climate-change effects on mountain glaciers: a pilot study with the European Alps, *Annals of Glaciology* , vol. 21, p. 206-212.

Haeberli, W. and M. Beniston. 1998. Climate change and its impacts on glaciers and permafrost in the Alps. *Ambio* 27, 258-265.

Hansen, J., R. Ruedy, J. Glascoe, and Mki. Sato 1999. GISS analysis of surface temperature change. *J. Geophys. Res.* 104, 30997-31022.

Hansen, J.E., R. Ruedy, Mki. Sato, M. Imhoff, W. Lawrence, D. Easterling, T. Peterson, and T. Karl 2001. A closer look at United States and global surface temperature change. J. Geophys. Res. 106, 23947-23963.

Harrison, W.D., 1972, Temperature of a temperate glacier: Journal of Glaciology, v.11, p. 15-29.

Harrison, W.D., 1972, Temperature measurement in a temperate glacier: Journal of Glaciology, v. 14, p. 23-30.

Hartmann, D. L., 1994, Global Physical Climatology, v.1 p. 9-10.

Hooke, R. B., 1977, Basal temperatures in polar ice sheets: a qualitative review: Quaternary Reseach, v. 7, p. 1-13.

Jiejun, L., 1986: Glaciers in Tibet, v. 6 p 130-140. (in Chinese).

Jiejun, L. and zhengxing, Z., 1986: Glaciers in Tibet, v. 6 p 217-231. (in Chinese).

Kang, X., 1996: The features of climate changes in the Qingzang Plateau area during the last 40 years. J. Glaciol. Geocryol. V. 18 p 280-288.

Landmark, B., 1996, Earth observation, v. 4 p.52-55.

Meier, M.F., 1984, Contribution of small glaciers to global sea level, *Science*, vol. 51, p. 49-62.

Mool, P.K., 2000, Inventory of Glaciers, Glacial Lakes and Glacial Lake Outburst Floods, v. 4 p.33-35.

MTAR., 1882, Meteorology in Tibet Autonomous Region 1951- 1980. v. 5 p 220-240. (in Chinese).

Muller, F., 1977, Instruction for Compilation and Assemblage of Data for a world Glacier Inventory.

Olseth, J. A., 1989, OBSERVED AND MODELLED HOURLY LUMINOUS EFFICACIES UNDER ARBITRARY CLOUDINESS, *Solar Energy* v. 42 p.221-233.

Olseth, J. A., 1993, CHARACTERISTICS OF HOURRLY GLOBAL IRRADIANCE MODELLED FROM CLOUD DATA, *Solar Energy* v. 51 p.197-204.

Olseth, J. A., 1996, ON THE ESTIMATION OF ATMOSPHERIC RADIATION FROM SURFACE METEOROLOGICAL DATA, *Solar Energy* v. 56 p.349-358.

Paterson, W. S. B., 1994, THE PHYSICS OF GLACIERS, v. 11 p. 238-245.

Paterson, W. S. B., 1994. THE PHYSICS OF GLACIERS, v. 4 p. 53-66.

Peterson, T. c., R. S. vose, R. Schmoyer, and V. Razuvaev, 1997, Quality Control of Monthly Climate Data: The GHCN Experience. Int. J. Climatol., submitted

Shengtang, Z., 1984, Lakes and Glaciers in Tibet, v. 10 p. 153-175. (in Chinese)

Wang, L., 2003, Climate variability over the Tibetan Plateau.

Warrick, R. A., C. L. Provost, M. F. Meier, J. Oerlemans, and P. L. Woodworth, 1996, Changes in sea level, in *Climate Change 1995: The Science of Climate Change*, 359-405,

Williams.R.S.,Jr, D.K Hall, 1997 Comparison of satellite-derived with ground-based measurements of the fluctuations of the margins of Vatnajökull, Iceland, 1973-92, Ann. Glaciol., 24, 72-80,

.

.

.

.

.